Numerical Simulations of Synthetic Ester Hydrolysis in the Indoor Environment

Do Young Maeng[1], *V. Faye McNeill*[1,2*]

[1]Department of Chemical Engineering, Columbia University, New York, NY USA 10027

[2]Department of Earth and Environmental Sciences, Columbia University, New York, NY USA 10027

*to whom correspondence should be addressed. vfm2103@columbia.edu

Abstract

The hydrolysis of synthetic esters (SEs), including phthalates and adipates, in damp indoor environments can lead to the release of volatile organic compounds implicated in poor air quality and acute health impacts, known as "sick building syndrome" (SBS). We have adapted the multiphase atmospheric chemistry box model, GAMMA, to simulate SE hydrolysis occurring in surface films in the indoor environment, along with multilayer boundary layer mass transfer and ventilation, in order to investigate this phenomenon on a process level. We then applied the model

to analyze three scenarios in which hydrolysis has been hypothesized to have a significant impact on indoor air quality. Simulation results suggest that: (1) alkaline hydrolysis of bis(2-ethylhexyl) adipate (DEHA) and bis(2-ethylhexyl) phthalate (DEHP) from PVC flooring on damp surfaces alone is not sufficient to explain the levels of 2-ethylhexanol reported in indoor air during episodes of SBS; (2) acute exposure to 2,2,4-trimethyl-1,3-pentanediol (TMPD) may be of concern during and shortly after the application of latex paint on an alkaline surface; and (3) alkaline hydrolysis of SEs following their airborne uptake in aqueous films is not expected to generate considerable amounts of alcohols associated with SBS.

Introduction

Hydrolysis has been identified as a potentially important indoor chemistry process, responsible for secondary emissions of several notable indoor pollutants.[1] In the context of indoor environment, it was first speculated as a source of volatile organic compounds (VOCs) in studies observing the effect of relative humidity on VOC emission from building products in the 1990s.[2,3] Since then, the discussion on hydrolysis in indoor air has gained attention due to its association with 2-ethylhexanol, the hydrolysis product of bis(2-ethylhexyl) phthalate (DEHP) and bis(2-ethylhexyl) adipate (DEHA). Incidents of asthma-like symptoms, referred to as "sick building syndrome" (SBS), have been reported following occupant exposure to 2-ethylhexanol, believed to be generated via hydrolysis of DEHP and DEHA found in polyvinylchloride (PVC) flooring.[4–7] While hydrolysis of synthetic esters (SEs)—such as DEHP and DEHA—is relatively slow even under alkaline conditions which may be present on concrete,[8–10] the ubiquitous nature of SEs in the indoor environment raises concerns about the possible contribution of these pathways to poor indoor air quality during both acute SBS episodes and more ordinary conditions. Recent studies

have also observed the presence of hydrolysis products of SEs in sampled household dust in the United States and East Asia, further suggesting the relevance of hydrolysis in typical indoor conditions.[11,12] Despite the increasing evidence that hydrolysis may be a source of volatile organic compounds (VOCs) indoors, the temporal evolution of VOCs from SE hydrolysis has not been investigated in relation to hydrolysis chemical kinetics and interphase mass transfer.

In order to investigate the possible effects of SE hydrolysis on indoor air quality, we adapted the multiphase atmospheric chemistry box model, GAMMA,[13] to numerically simulate SE hydrolysis occurring in surface aqueous films in the indoor environment, including mass transfer from the surface, through the boundary layer, into the room air (breathing zone). We call this new model GAMMA-Chemistry of the Indoor Environment (GAMMA-CIE). We tested three scenarios in which hydrolysis has been hypothesized to impact indoor air quality: (1) installation of PVC flooring on damp concrete, resulting in hydrolysis of bis(2-ethylhexyl) adipate (DEHA) and bis(2-ethylhexyl) phthalate (DEHP);[5,14] (2) application of latex paint on concrete, resulting in hydrolysis of 2,2,4-trimethyl-1,3-pentanediol monoisobutyrate (TMPD-MIB);[15,16] and (3) gas-phase SE uptake by surface aqueous film in contact with concrete, resulting in hydrolysis of common phthalate esters (PEs) and phosphorus flame retardants (PFRs).[17–19] The generation of gas-phase 2-ethylhexanol (2-EH), 2,2,4-trimethyl-1,3-pentanediol (TMPD), and other semi-volatile and volatile organic compounds (SVOCs and VOCs) from the aforementioned hydrolysis reactions was simulated and compared to literature data.

Methods

GAMMA-CIE. Following McNeill et al. (2012), GAMMA-CIE consists of 784 coupled differential equations describing the temporal evolution of parent SE compounds undergoing hydrolysis reactions and the formation of reaction products in the aqueous phase, mass transfer between gas phase and aqueous phase, and gas-phase oxidation.[13] GAMMA-CIE runs on a personal computer in the MATLAB environment using the `ode15s` stiff solver.

In GAMMA, the aqueous phase consists of spherical aqueous aerosol or cloud droplets suspended in air. In GAMMA-CIE, the aqueous phase consists of a flat aqueous film in direct contact with an indoor surface instead. As such, the mass transfer scheme following Schwartz (1986) was modified to account for diffusion through the gas-phase boundary layer and mixing into the room air by adopting the multi-layer approach described by Shiraiwa et al. (2010) and Morrison et al. (2019).[20–22] Figure 1 illustrates the general schematic of GAMMA-CIE below.

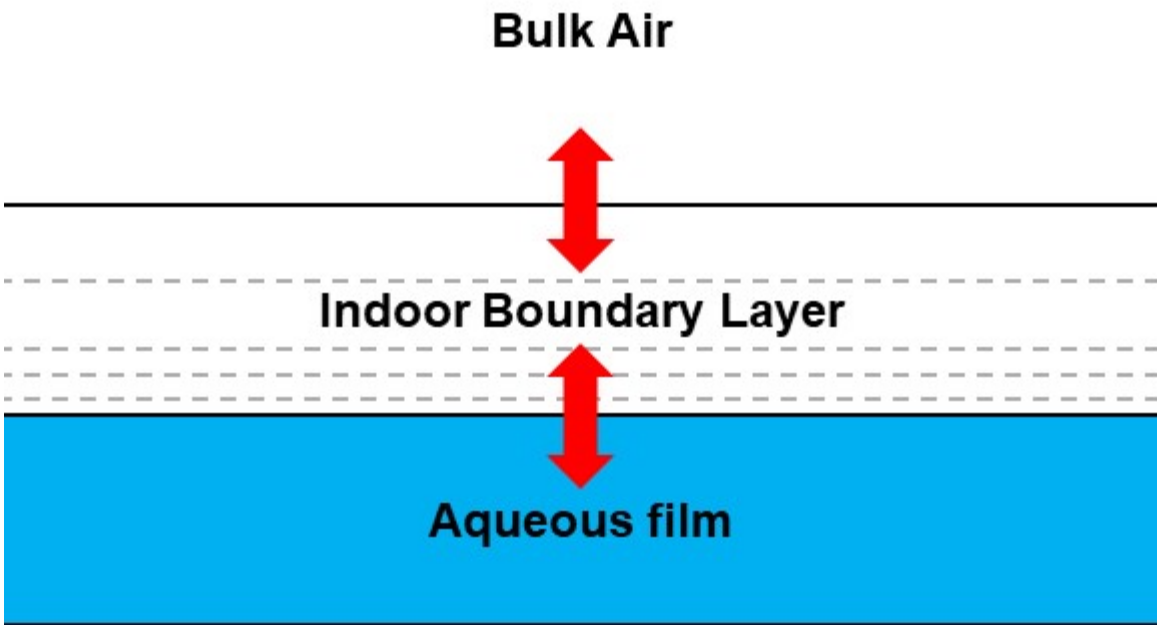

Figure 1. GAMMA-CIE model schematic. As described in Equations 1 through 4, the model considers reaction kinetics and mass transfer for each layer. Additionally, loss by ventilation is also taken into account for the bulk air layer.

The concentration of a species *i* in the bulk gas phase and the boundary layer, separated into *n* layers with the *n*th layer as the bottommost, is described by the set of equations below:

$$\frac{dP_{i,bulk}}{dt} = \left(P_{i,1} - P_{i,bulk}\right)\left(\frac{D_{g,i,bulk,1}}{d_{bulk,1}}\right)\left(\frac{A_{bulk}}{V_{bulk}}\right) + \sum_j r_{ij,gas} - ACH \cdot P_{i,bulk} \quad (1)$$

$$\frac{dP_{i,1}}{dt} = \left(P_{i,bulk} - P_{i,1}\right)\left(\frac{D_{g,i,bulk,1}}{d_{bulk,1}}\right)\left(\frac{A_1}{V_1}\right) + \left(P_{i,2} - P_{i,1}\right)\left(\frac{D_{g,i,1,2}}{d_{1,2}}\right)\left(\frac{A_1}{V_1}\right) + \sum_j r_{ij,gas} \quad (2)$$

$$\frac{dP_{i,k}}{dt} = \left(P_{i,k-1} - P_{i,k}\right)\left(\frac{D_{g,i,k-1,k}}{d_{k-1,k}}\right)\left(\frac{A_k}{V_k}\right) + \left(P_{i,k+1} - P_{i,k}\right)\left(\frac{D_{g,i,k,k+1}}{d_{1,2}}\right)\left(\frac{A_k}{V_k}\right) + \sum_j r_{ij,gas} \quad (3)$$

$$\frac{dP_{i,n}}{dt} = \left(P_{i,n-1} - P_{i,n}\right)\left(\frac{D_{g,i,n-1,n}}{d_{n-1,n}}\right)\left(\frac{A_n}{V_n}\right) + k_{mt,i}a_L\left(\frac{C_i}{H_i^*} - P_{i,n}\right) + \sum_j r_{ij,gas} \quad (4)$$

where layers k = 2, 3, …, n-1, P_i is the partial pressure of species i, $D_{g,i}$ is the gas-phase diffusion coefficient of species i, d is the average travel distance (equivalent to the mean thickness of the two participating layers), A_k and V_k are the surface area and volume of layer k, respectively, ACH is the air changes per hour (i.e., ventilation rate) in the given indoor space, $r_{ij,gas}$ is the rate of gas-phase reaction j that species i participates in, $k_{mt,i}$ is the gas-aqueous mass transfer coefficient for species i, a_L is the aqueous liquid fraction ($cm^3\ cm^{-3}$), C_i is the aqueous-phase concentration of species i, and H_i^* is the effective Henry's Law constant of species i. The gas-phase diffusion coefficient, $D_{g,i}$, factors in both molecular diffusion and eddy diffusion as shown by the equation below:[23]

$$D_{g,i} = D_{m,i} + D_{e,i} \tag{5}$$

where $D_{m,i}$ is the molecular diffusion coefficient of species i, and $D_{e,i}$ is the eddy diffusion coefficient at height y above the aqueous film given by

$$D_{e,i} = K_e y^2 \tag{6}$$

where K_e is the turbulence intensity, varying from 0.1 to 10 s^{-1}.[24] $D_{e,i}$ was evaluated at the height corresponding to the boundary between two participating layers.

The gas-aqueous mass transfer coefficient, $k_{mt,i}$, and aqueous liquid fraction, a_L, have been adjusted from Schwartz (1986) to accommodate for an indoor aqueous film instead of an aqueous aerosol particle in the atmosphere. $k_{mt,i}$ and a_L are now expressed as follows:[19]

$$k_{mt,i} = \frac{1}{\frac{\delta_n \delta_{film}}{D_{m,i}} + \frac{4\delta_{film}}{\omega_i \alpha_i}} \tag{7}$$

$$a_L = \frac{\delta_{film}}{\delta_{film} + \delta_n} \tag{8}$$

where δ_n is the bottommost gas-phase layer thickness, δ_{film} is the aqueous film thickness, ω_i is the

thermal velocity of species *i*, and α_i is the accommodation coefficient of species *i*. Data on gas-aqueous accommodation coefficients for these species are not available, so they were all assigned values of 0.02, which is representative of the uptake of semi-volatile organic compounds to aqueous surfaces.[25]

The aqueous-phase concentration of a species *i* is shown below:

$$\frac{dC_i}{dt} = \frac{k_{mt,i}}{\mathbf{R}T}\left(P_{i,n} - \frac{C_i}{H_i^*}\right) + \sum_k r_{ik,aq} \quad (9)$$

where **R** is the gas constant and *T* is temperature. Further details on the model parameters, gas- and aqueous-phase reactions, boundary layer characterization, effective Henry's Law constant calculation, and mass transfer coefficient derivation can be found in the Supporting Information.

Gas-Phase Chemistry. Consumption of gas-phase SEs and their hydrolysis products by hydroxyl radical (OH) oxidation is considered in the model. Oxidation kinetics data were only available for certain phthalate and alcohol species.[26,27] For species with missing kinetics data, rate constants were estimated using structure-activity relationships (EPI Suite AOPWIN).[28] OH concentrations in indoor air are predicted to vary approximately between 1×10^5 and 4×10^5 molecules cm^{-3},[29] depending primarily on the rates of chemical production (e.g., terpene ozonolysis, nitrous acid photolysis) and consumption (e.g., OH reactions with organics).[22,30] For SVOCs and VOCs of interest in this study, their loss by OH oxidation was much slower than their removal by ventilation as noted by the timescales of these two processes in the Supporting Information, so OH concentration was treated as a constant at 4×10^5 molecules cm^{-3}. All OH oxidation reactions and their rate constants in GAMMA-CIE are listed in Table S3.

Aqueous-Phase Chemistry. Alkaline hydrolysis of esters (R'COOR) drives the production of acids and alcohols predicted in this study. The simplified reaction equation is illustrated below:[31]

$$R'COOR + OH^- \rightarrow R'COO^- + ROH \qquad (R1)$$

where R'COO- is the deprotonated acid or lower-order ester, and ROH is the alcohol. The rate of this second-order reaction is pH dependent as described by the following:

$$r_{hydrolysis} = k[R'COOR][OH^-] \qquad (10)$$

where *k* is the alkaline hydrolysis second-order rate constant. Multiple studies have investigated the hydrolysis kinetics of esters abundant in the indoor environment,[8–10,32] but for the hydrolysis of lower-order esters for which experimental data are not available, EPI Suite HYDROWIN estimations were used instead.[28] Species are grouped by their relevant hydrolysis cascade reactions in Table 1 for a general overview on the three aforementioned scenarios. Complete list of hydrolysis reactions can be found in Table S4.

Table 1. List of Parent SEs and Hydrolysis Products

Scenario #	Parent Ester	Hydrolysis Product Lower-Order Ester	Alcohol/Acid
1	Bis(2-ethylhexyl) adipate (DEHA)	Mono(2-ethylhexyl) adipate (MEHA)	2-Ethylhexanol (2-EH) Adipic acid (AA)
1	Bis(2-ethylhexyl) phthalate (DEHP)	Mono(2-ethylhexyl) phthalate (MEHP)	2-Ethylhexanol (2-EH) Phthalic acid (PA)
2	2,2,4-Trimethyl-1,3-pentanediol monoisobutyrate (TMPD-MIB)	*N/A*	2,2,4-Trimethyl-1,3-pentanediol (TMPD) Isobutyric acid (IBA)
3	Diethyl phthalate (DEP)	Monoethyl phthalate (MEP)	Ethanol (EtOH) Phthalic acid (PA)

3	Diisobutyl phthalate (DIBP)	Monoisobutyl phthalate (MIBP)	Isobutanol (*i*-BuOH) Phthalic acid (PA)
3	Dibutyl phthalate (DBP)	Monobutyl phthalate (MBP)	Butanol (BuOH) Phthalic acid (PA)
3	Benzyl butyl phthalate (BBzP)	Monobenzyl phthalate (MBzP) Monobutyl phthalate (MBP)	Benzyl alcohol (BnOH) Butanol (BuOH) Phthalic acid (PA)
3	Tris(2-chloroethyl) phosphate (TCEP)	Bis(2-chloroethyl) phosphate (BCEP)	2-chloroethanol (2-CE)
3	Tris (1-chloro-2-propyl) phosphate (TCIPP)	Bis(1-chloro-2-propyl) phosphate (BCIPP)	1-chloro-2-propanol (1C2P)

Test Conditions. For all case studies, the temperature was set to 25 °C to represent typical room temperature. The aqueous film was assumed to be a rectangular layer in contact with an alkaline surface (e.g., concrete), resulting in the migration of hydroxide ions from the surface to the aqueous film.[33] Therefore, the pH of the aqueous film was varied between 10 and 13—pH range observed on screed or young concrete surfaces[5,33,34]—and was held constant throughout each simulation (i.e., rate of consumption of hydroxide ion by hydrolysis was considered negligible compared to its rate of migration from concrete to the film). Ventilation rate was varied between 0.5 and 5.5 ACH to account for different locations, from naturally ventilated homes with relatively low ACH to mechanically ventilated buildings with relatively high ACH.[35–37] Further details on the following test conditions specific to individual scenarios are provided in the Supporting Information.

Scenario 1: Hydrolysis of DEHA and DEHP

DEHA and DEHP were assumed to be present in excess in the surface material (e.g., PVC flooring), leading to an instantaneous migration of DEHA and DEHP from the surface into the aqueous film (i.e., DEHA and DEHP concentrations were treated as constants at the aqueous solubility limit). The reported water solubilities of DEHP varied by two orders of magnitude in literature,[38,39] so both low- and high-DEHP solubility conditions were considered in this study. There are uncertainties regarding the thickness of the aqueous film, which is affected by several factors such as the chemical composition of the film, hygroscopicity of the surface, and relative humidity (RH).[40] Schwartz-Narbonne & Donaldson (2019) measured water uptake varying in the range of 1–5 μg/cm^2 at RH > 60%, equivalent to 10-50 nm in thickness assuming a layer of even thickness with density of pure water.[41] To simulate the upper bound of hydrolysis activity, however, we assumed film thickness to be 1 μm which may be plausible in consideration of conditions favorable for water adsorption on indoor surfaces.[42] Sensitivity of gas-phase evolution to film thickness is reported in the Supporting Information. Bulk air dilution factor of 0.4 m^{-1} was used in consideration of standard indoor floor-to-volume ratio.[43] Simulated time of 12 h was sufficient for DEHA, DEHP, MEHA, MEHP, and 2-EH concentrations to reach steady state as shown in Figures S2 through S5.

Scenario 2: Hydrolysis of TMPD-MIB

The whole latex paint film was treated as an aqueous film in which a finite amount of the parent ester TMPD-MIB hydrolyzes over time. Thus, the film thickness was set to 100 μm to represent a typical paint film, and the initial aqueous-phase TMPD-MIB concentration was based on the mass

composition in latex paint.[15] The bulk air dilution factor was set to 1.3 m^{-1} in consideration of the ubiquity of painted surfaces in indoor environments.[44] The process was simulated for a shorter period of 8 h to analyze short-term exposure to TMPD, one of the hydrolysis products of TMPD-MIB, during the phase in which the paint would be wet.

Scenario 3: Hydrolysis of Common PEs and PFRs

In this case study, the bulk gas-phase layer acted as an infinite reservoir of PEs and PFRs found in appreciable amounts in indoor air. PE and PFR concentrations were treated as constants at their reported airborne measurements from Bergh et al. (2011) listed in Table S7,[19] and the resulting uptake of airborne PEs and PFRs was the only source of parent esters in the aqueous film. The airborne measurements used in the model are sums of gas and particulate phases, but they are treated as gas-phase concentrations because they are known to be present predominantly in the gas phase.[17] Film thickness of 1 μm and bulk air dilution factor of 0.4 m^{-1} were used to consider an aqueous film trapped below the flooring. pH and ACH were at fixed values of 13 and 0.5 ACH, respectively, to target the maximum predictable gas-phase concentrations of the hydrolysis product species. The simulation time was extended to 300 h for all species.

Results & Discussion

Tables 2, 3 and 4 summarize the GAMMA-CIE predicted concentrations of gas-phase species in comparison to their respective field measurements in literature for scenarios 1 to 3, respectively. In-depth discussion on the simulation results for each scenario is elaborated below.

Table 2. Predicted and Measured Gas-Phase Concentrations (μg/m^3) of Species in Scenario 1: Hydrolysis of DEHA and DEHP

Name	GAMMA-CIE[a] (μg/m^3)	Reported Indoor Levels (μg/m^3)	Reference
Bis(2-ethylhexyl) adipate[b] (DEHA)	0.0016	0.005–0.015	Weschler and Nazaroff (2008)[17]
Bis(2-ethylhexyl) phthalate (DEHP)	0.095–20	<2.253	Fromme et al. (2004)[45]
Mono(2-ethylhexyl) adipate[b] (MEHA)	4.1×10^{-7}	*N/A*	*N/A*
Mono(2-ethylhexyl) phthalate (MEHP)	1.8×10^{-8}–3.8×10^{-6}	*N/A*	*N/A*
2-Ethylhexanol (2-EH)	4.7×10^{-6}–1.2×10^{-4}	0.3–1000+	Wakayama et al. (2019)[14]
Phthalic acid (PA)	*N/A*[c]	*N/A*	*N/A*
Adipic acid[b] (AA)	*N/A*[c]	*N/A*	*N/A*

[a]Steady-state concentrations. Simulation conditions were pH 13 and 0.5 ACH for low- and high-DEHP conditions.
[b]DEHA, MEHA, and AA are not affected by DEHP saturation condition, thus only having a single predicted value.
[c]Negligible concentrations of ~10^{-20} μg/m^3 were predicted for PA and AA.

Table 3. Predicted and Measured Gas-Phase Concentrations (μg/m^3) of Species in Scenario 2: Hydrolysis of TMPD-MIB

Name	GAMMA-CIE (μg/m^3)	Reported Indoor Levels (μg/m^3)	Reference
2,2,4-Trimethyl-1,3-pentanediol monoisobutyrate (TMPD-MIB)	810[a]	1680[b]	Norbäck et al. (1995)[46]
2,2,4-Trimethyl-1,3-pentanediol (TMPD)	240[c]	*N/A*	*N/A*
Isobutyric acid (IBA)	2.6×10^{-4}[d]	*N/A*	*N/A*

[a]Peak concentration during simulation time of 8 h. Simulation conditions were pH 10 and 0.5 ACH.
[b]Maximum exposure level measured during a 1 h house painting session.
[c]Peak concentration during simulation time of 8 h. Simulation conditions were pH 13 and 0.5 ACH.
[d]Steady state concentration after simulation time of 8 h. Simulation conditions were pH 10 and 0.5 ACH.

Table 4. Predicted and Measured Gas-Phase Concentrations (μg/m^3) of Species in Scenario 3: Hydrolysis of Common PEs and PFRs

Name	GAMMA-CIE (μg/m^3)	Reported Indoor Levels (μg/m^3)	Reference
Monoethyl phthalate (MEP)	3.9×10^{-6}	*N/A*	*N/A*
Monoisobutyl phthalate (MIBP)	8.7×10^{-8}	*N/A*	*N/A*
Monobutyl phthalate (MBP)	1.4×10^{-6}	*N/A*	*N/A*
Monobenzyl phthalate (MBzP)	5.1×10^{-10}	*N/A*	*N/A*
Bis(2-chloroethyl) phosphate (BCEP)	2.2×10^{-7}	*N/A*	*N/A*
Bis(1-chloro-2-propyl) phosphate (BCIPP)	2.1×10^{-9}	*N/A*	*N/A*
Ethanol (EtOH)	3.7×10^{-4}	49–2787[a]	Gallego et al. (2009)[47]
Isobutanol (*i*-BuOH)	3.2×10^{-6}	1–<5[b]	Brown et al. (1994)[48]

Butanol (BuOH)	6.6×10^{-5}	14–95[a]	Gallego et al. (2009)[47]
Benzyl alcohol (BnOH)	3.1×10^{-5}	864–5446[c]	Gerster et al. (2014)[49]
2-Chloroethanol (2-CE)	6.8×10^{-8}	*N/A*	*N/A*
1-Chloro-2-propanol (1C2P)	6.8×10^{-10}	*N/A*	*N/A*
Phthalic acid (PA)	*N/A*[d]	*N/A*	*N/A*

[a]During an odor episode in several locations of a single apartment dwelling.
[b]In established dwellings.
[c]During cleaning activities.
[d]Negligible concentrations of ~10^{-21} μg/m^3 were predicted for PA.

Scenario 1: Hydrolysis of DEHA and DEHP

Gas-phase parent ester DEHP equilibrated at 0.095 and 20 μg/m^3 at low- and high-DEHP conditions, respectively, as noted in Table 2. Reported mean concentrations of gas-phase DEHP ranged between 191 and 599 ng/m^3 with a maximum of 2253 ng/m^3,[45] implying overabundance of DEHP in the high-DEHP condition simulation and, on the contrary, underestimation of DEHP in low-DEHP condition simulation. Therefore, the predicted concentrations of the following hydrolysis products at low- and high-DEHP conditions should be interpreted as the lower and upper bounds in this scenario. The predicted gas-phase concentration of the other parent ester, DEHA, was 1.6 ng/m^3, which is close to the measured average range of 5 and 15 ng/m^3, indicating that the DEHA saturation assumption was appropriate.

As noted in Table 2, negligible amounts of gas-phase PA and AA were generated in the simulation at all pH and ACH values. The rate of interphase transport for PA and AA is significantly slower than other species because of their high effective Henry's law constant, which is pH dependent for organic acids. In such highly basic conditions where the acids are in their deprotonated form, the acids tend to remain in the aqueous phase.[50–52] The effective Henry's law constants for PA, AA, and IBA at pH 10 and 13 are greater than their intrinsic counterparts by

several orders of magnitude, as shown in Table S9. While the slow interphase transport is responsible for the predicted negligible gas-phase concentrations of PA and AA, control simulations performed with lower arbitrary values of Henry's law constant assigned to both species for faster mass transport suggest that the slow hydrolysis kinetics and overall low water solubilities of parent esters (DEHA and DEHP) would limit the gas-phase generation of PA and AA to low levels of ~10^{-5} μg/m^3.

Gas-phase 2-EH generation was simulated with varying pH and ACH to understand the effect of those parameters on the overall process, as illustrated in Figure 2. Increase in aqueous film pH by 1 (in the range 10-13) resulted in a proportional increase in 2-EH concentrations by a factor of approximately 10 for both low- and high-DEHP cases. It is apparent that the aqueous film pH, and consequently the indoor surface pH, is a key parameter in SE degradation by hydrolysis. Changes in ACH were most effective at low ventilation conditions, decreasing the predicted 2-EH concentrations by a factor of 3 when increasing from 0.5 to 1.5 ACH. Overall, the predicted levels of 2-EH were significantly lower than reported indoor values from the literature (Table 2). At pH 13, 0.5 ACH, and high-DEHP saturation condition, GAMMA-CIE predicted 1.2×10^{-4} μg/m^3 of gas-phase 2-EH, which is approximately 7 orders of magnitude lower than the upper bound of measured concentrations of ~1000 μg/m^3 in extreme SBS cases.[14]

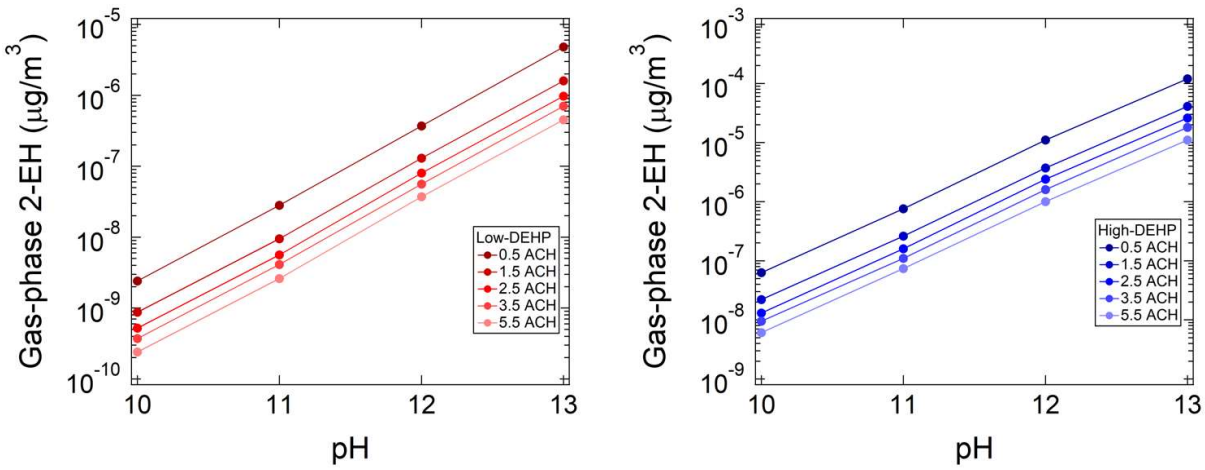

Figure 2. Predicted gas-phase 2-EH concentrations with varying aqueous film pH and ACH at low-DEHP (left) and high-DEHP (right) conditions.

Simulation results suggested that hydrolysis of DEHA and DEHP from PVC flooring would not produce gas-phase 2-EH at levels comparable to values measured during SBS incidents. Therefore, we hypothesized that an unknown, non-hydrolysis process (e.g., biotic degradation[53]) may be active in degrading DEHA and DEHP and their lower-order esters to produce 2-EH. To determine the magnitude of discrepancy between the hydrolysis kinetics and the mechanism necessary to produce gas-phase 2-EH concentrations observed in field studies, a hypothetical first-order aqueous degradation process was considered for DEHA, DEHP, MEHA, and MEHP under hydrolysis-ideal conditions of pH 13, 0.5 ACH, and high-DEHP saturation. The rate of this hypothetical process was adjusted by trial and error to produce steady-state gas-phase 2-EH concentration of 2 μg/m^3, emulating the observations of 1–4 μg/m^3 of gas-phase 2-EH during an incidence of SBS.[14] The hypothetical process was accelerated to 0.2 s^{-1} to produce gas-phase 2-EH concentration of 2 μg/m^3 as depicted by Figure 3 below. This rate is approximately 2 to 4 orders of magnitude faster than that of alkaline hydrolysis at pH 13. The difference in magnitude

between the hypothetical process and alkaline hydrolysis could be even greater when considering 2-EH concentrations of ~1000 μg/m^3 was observed in certain episodes.

There are several possible explanations for the observed discrepancy. As noted above, biotic degradation by bacteria, yeast, and fungi could be a relevant process with a rate higher or comparable to that of abiotic hydrolysis at high relative humidity.[11,53] Another reason could be the acceleration of reaction kinetics in microfilms, where the partial solvation of the reactants leads to a lower activation barrier and higher reactivity, notably for reactions such as hydrolysis involving an attack at the carbonyl carbon.[54,55] Wei et al. (2020) suggests a hundredfold increase in the intrinsic reactivity from bulk-phase reaction to partially solvated reaction, which roughly corresponds to the magnitude of difference observed in our hypothetical rate constant. However, this effect has yet to be confirmed with further experimental data, specifically for the hydrolysis of SEs. Lastly, hydrolysis of acrylate and acetate copolymers in adhesives could be the dominant source instead, which is evident in emission studies but warrants further research on the reaction kinetics and adequate reaction systems for modeling purposes.[5,56,57]

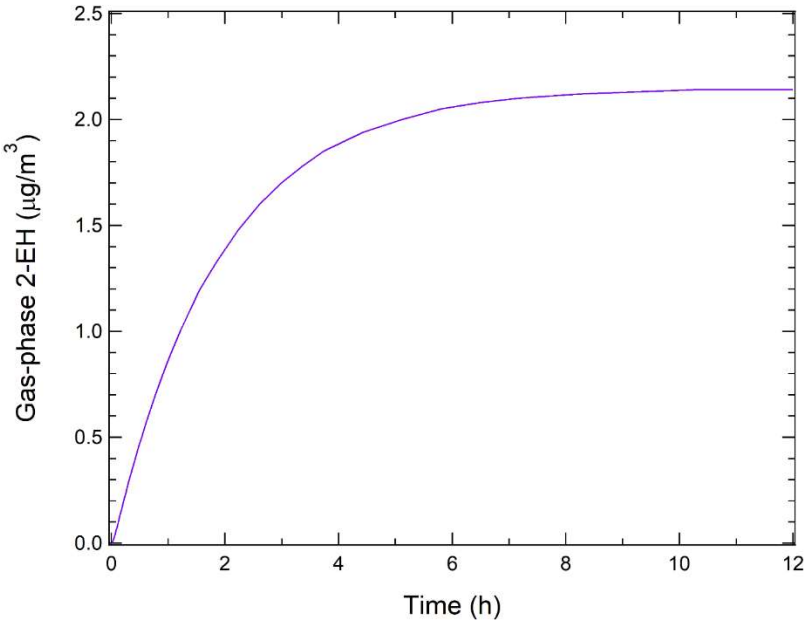

Figure 3. Predicted concentration profile of gas-phase 2-EH at aqueous film pH 13, 0.5 ACH, and high-DEHP condition, with the addition of a first-order hypothetical degradation process of 0.2 s^{-1} for aqueous-phase DEHA, DEHP, MEHA, and MEHP. See text for details.

Scenario 2: Hydrolysis of TMPD-MIB

Figure 4 below illustrates the concentration profile of gas-phase parent ester TMPD-MIB over simulation time of 8 h at pH 10 and 0.5 ACH with a peak concentration of 810 μg/m^3 at t = 0.6 h. Decreasing the film basicity to below pH 10 in GAMMA-CIE had a negligible increase on this predicted gas-phase peak concentration, most likely because the rate of interphase transport was already significantly faster than that of TMPD-MIB consumption by hydrolysis at pH 10. Field studies on SVOC emissions following latex paint application measured TMPD-MIB peak concentrations of approximately 1~1.7 mg/m^3, comparable to the predicted peak considering that simulations were performed assuming a smaller TMPD-MIB content of 0.67% in paint than that of 1.35% in paint used by Sparks et al. (1999).[46,58] The trend is also similar between the

concentration profile predicted by GAMMA-CIE in Figure 4 and those observed in experiments,[58,59] overall indicating good agreement on TMPD-MIB emission between model prediction and experimental measurements.

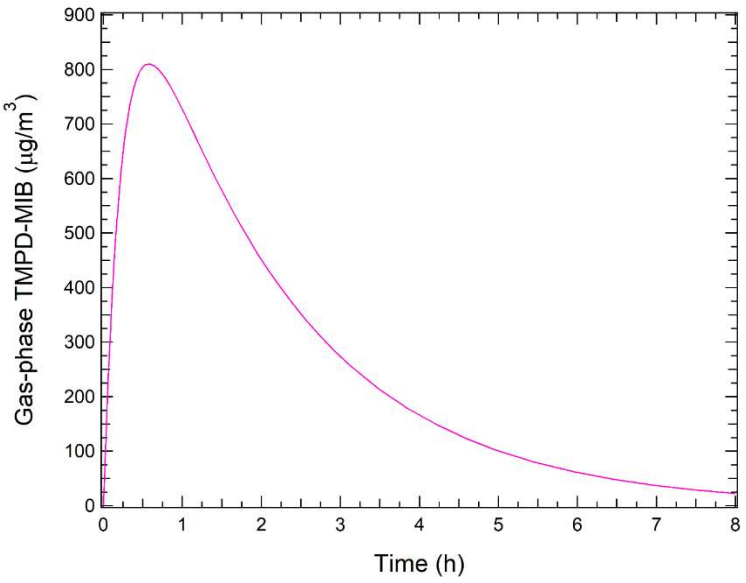

Figure 4. Predicted concentration profile of gas-phase TMPD-MIB at aqueous film pH 10 and 0.5 ACH with peak value of 810 µg/m^3.

The time evolution of gas-phase TMPD over simulation time of 8 h at varying film pH and low- and high-ACH conditions is shown in Figure 5. The predicted peak concentrations of TMPD at pH 13 were 240 µg/m^3 at t = 0.6 h for 0.5 ACH and 110 µg/m^3 at t = 0.3 h for 5.5 ACH. pH was the most influential factor in gas-phase evolution of TMPD, with near tenfold decrease in peak gas-phase concentrations per unit decrease in pH.

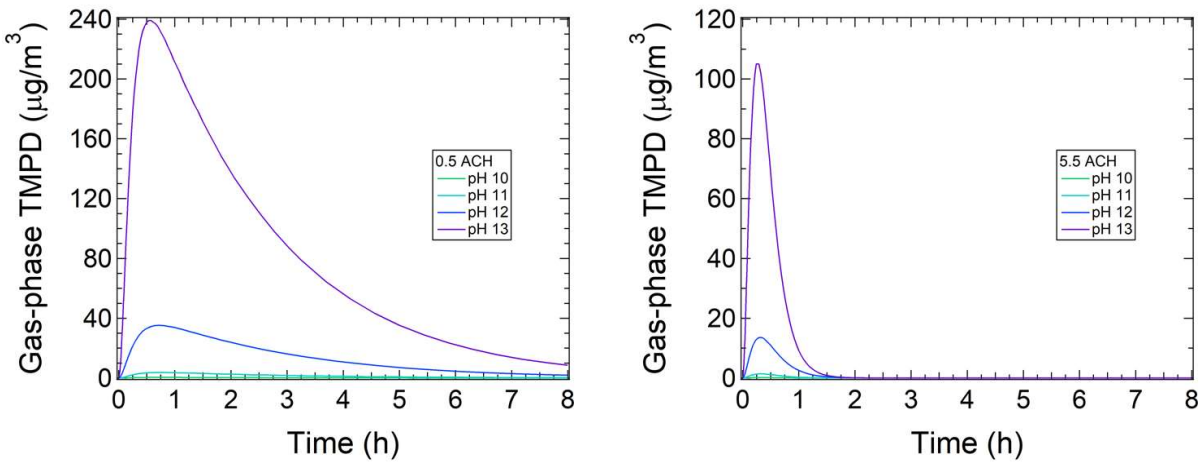

Figure 5. Predicted concentration profile of gas-phase TMPD with varying aqueous film pH at low-ACH (left) and high-ACH (right) conditions.

In contrast to TMPD-MIB and TMPD simulation results, GAMMA-CIE predicted much lower production of gas-phase IBA, rate-limited by the interphase mass transport from the high effective Henry's law constant. The predicted gas-phase concentration profile of IBA in Figure 6 below is distinctly different from those of TMPD-MIB and TMPD. Highest predicted concentration of gas-phase IBA was 2.6×10^{-4} μg/m^3 for 0.5 ACH and pH 10. As previously mentioned in the discussion of Scenario 1, higher pH conditions are associated with inhibition of interphase mass transport for acids such as IBA, resulting in an opposite trend compared to TMPD above. Similar to the gas-phase 2-EH concentrations in Scenario 1, increase in ventilation from 0.5 to 5.5 ACH resulted in a tenfold decrease in the predicted gas-phase IBA concentrations across all pH values. Accumulation of IBA in the aqueous phase was observed as shown in Figure 7 due to the slow partitioning process, with aqueous IBA concentration predicted to reach 0.018 M in the film at pH 13. Because IBA is a relatively weak acid, such concentrations are still not sufficient enough to significantly lower the pH of the film on its own. With the uptake of acidic gases indoors, however,

it may be possible that this build-up of aqueous IBA may partition into the gas phase as the film is acidified. Further discussion on indoor acids can be found in the Indoor Environment Implications section below.

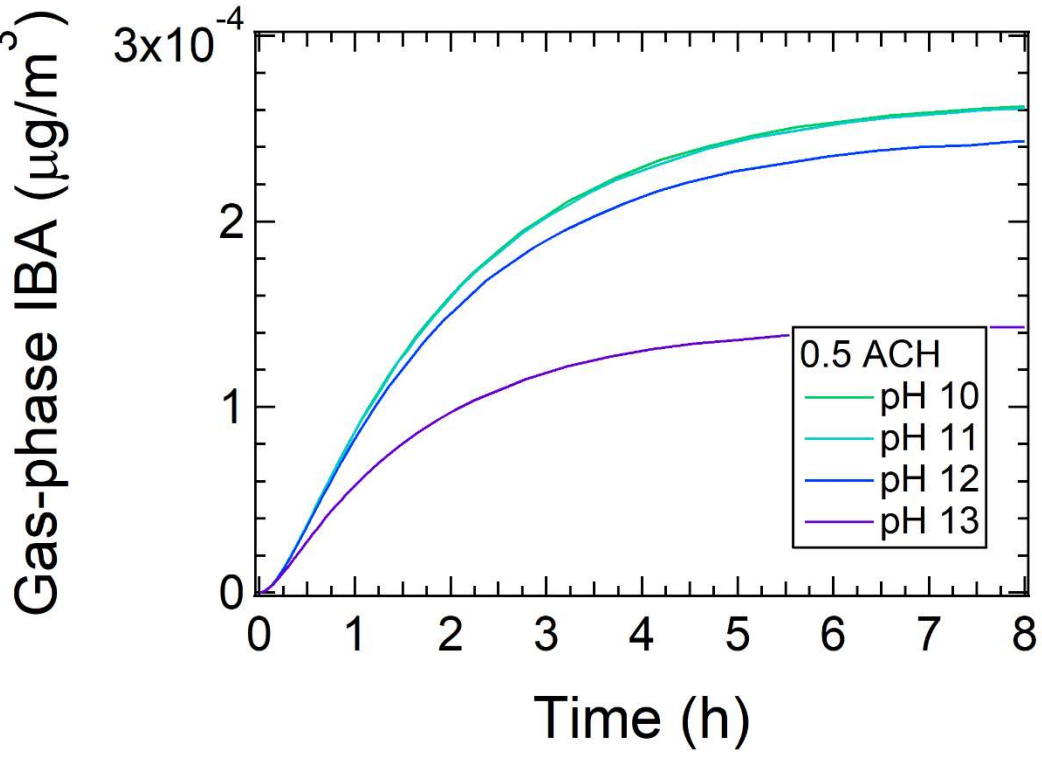

Figure 6. Predicted concentration profile of gas-phase IBA with varying aqueous film pH at low-ACH condition.

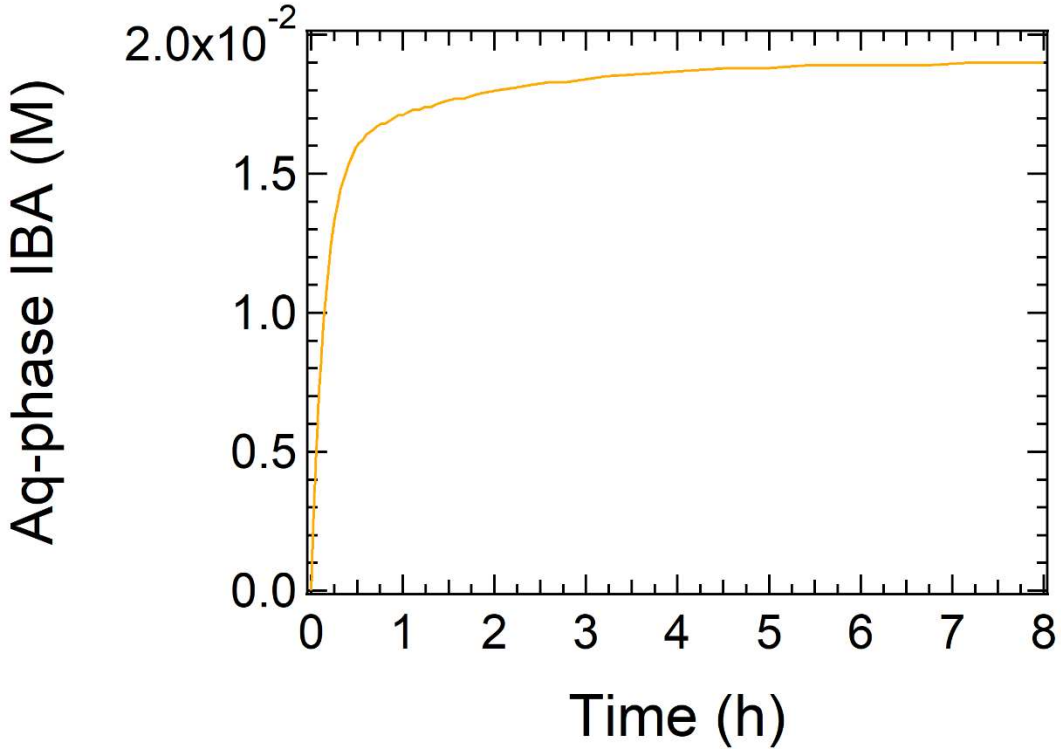

Figure 7. Predicted concentration profile of aqueous-phase IBA with at pH 13 and low-ACH condition.

Our predictions indicate that building occupants and interior painters may be exposed to high levels of irritants TMPD-MIB and its hydrolysis product TMPD during paintwork and shortly after its completion, especially in newly constructed buildings with high pH surfaces. Data on the indoor measurements and exposure limits of TMPD-MIB and TMPD are lacking, but both species are reported to cause irritation in the eyes, nose, skin, and respiratory tract.[60] Experimental data on the emissions of TMPD in paint applications would further validate the predicted results of this scenario.

Scenario 3: Hydrolysis of Common PEs and PFRs

The predicted gas-phase concentrations of SVOCs and VOCs under ideal hydrolytic degradation conditions are plotted in Figure 8 below. Among the lower-order esters, BCEP and BCIPP equilibrated more slowly than the other SVOCs primarily because they are the only lower-order

esters stable to hydrolysis in the system. MEP and MBP were the most abundant species due to their high parent ester concentrations shown in Table S7 and relatively fast rate of production by hydrolysis. Even so, predicted secondary emissions of SVOCs from the airborne SE uptake and the ensuing hydrolysis were of negligible amounts, not exceeding 10^{-5} μg/m^3.

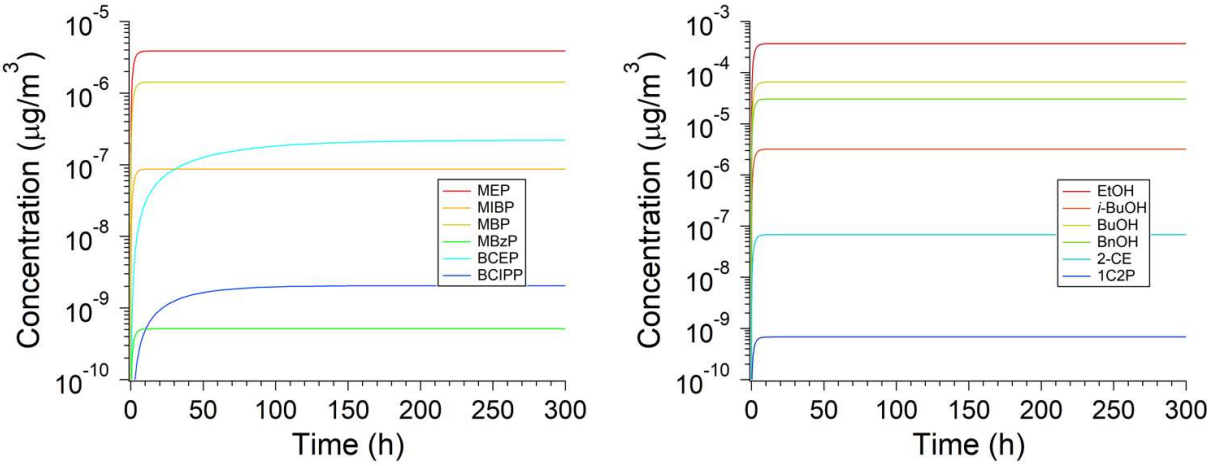

Figure 8. Predicted gas-phase concentration profile of SVOCs (left) and alcohols (right) at aqueous film pH 13 and 0.5 ACH.

Table 4 presents the predicted steady state concentrations in comparison to measured indoor concentrations of VOCs simulated in this study. It is apparent that the model predictions are several orders of magnitude smaller than the reported measurements for the alcohol species with available field data. This was expected since the reference values were collected during specific occasions (e.g., cleaning activities, odor episodes), likely affected by external (outdoor) sources, primary emissions, and other secondary processes,[47,56,61,62] which are non-analogous to the simulation scenario of generalized airborne SE uptake by the aqueous film on an alkaline surface. Even so,

the notable differences in the simulated concentrations and reported field concentrations suggest that hydrolysis from uptake of airborne SEs is not a significant contributor of indoor acids and alcohols in the proposed scenario. The uptake of airborne SE by aqueous films on indoor surfaces warrants further investigation, however, as the airborne concentrations of SEs may differ significantly depending on the presence of SE-rich objects at the location of interest. Additionally, it has been reported that substantial amounts of SEs can also be present in settled dust on indoor surfaces which have not been considered in this study,[17,19] so there may be greater amounts of parent SEs susceptible to degradation in this uptake process simulated in Scenario 3.

Indoor Environment Implications

This study employs a detailed multiphase chemistry model to quantitatively determine the development of gas-phase pollutants from indoor surface hydrolysis. We have used GAMMA-CIE in three indoor scenarios relevant to hydrolysis, but the applicability of the model can extend further to other indoor conditions, especially as information on indoor surface films becomes more available. In this following section, we discuss uncertainties and limitations in the model to be considered in extending the scope of the model.

The indoor film is likely comprised of various organic and inorganic species—namely aliphatic and aromatic hydrocarbons, carbohydrates, metals, sulfates, and nitrates—emitted from building occupants and different indoor activities.[18,63] Acknowledgement of such complex chemical composition introduces several possible factors which could be considered: indoor film water content, aqueous-organic phase separation and phase equilibria, heterogeneous reaction, ionic strength, and so on.

For the alkaline hydrolysis of SEs, we have only considered specific base catalyzed hydrolysis because it is presumably the dominant mechanism in presence of high calcium hydroxide

concentrations from fresh concrete. However, if other indoor bases, such as ammonia, nicotine, and inorganic and organic amines,[64] are transported into the aqueous film, then the organic esters may also degrade by general base catalyzed hydrolysis.[65–68] There are no studies on the general base catalyzed hydrolysis for SEs considered in our model, but this alternate degradation mechanism may be of importance in other indoor scenarios with high concentrations of indoor bases absorbed by the film.

Similar to the uptake of indoor bases mentioned above, uptake of acids may occur as there are several acids found indoors, such as carbon dioxide, nitric acid, sulfuric acid, and acetic acid.[64] In such instances, SEs may degrade by acid hydrolysis instead.[31,69] At the time of this study, experimental data on the kinetics of SE acid hydrolysis are unavailable, and the EPI Suite HYDROWIN is only able to estimate alkaline hydrolysis rate constants. Although acid hydrolysis is known to be generally slower than alkaline hydrolysis,[31] kinetic measurements on SE acid hydrolysis may open up the possibility of simulating common indoor scenarios which have not been explored yet.

Acknowledgements

We acknowledge the Alfred P. Sloan Foundation Chemistry of the Indoor Environment program for funding and Glenn Morrison and Manabu Shiraiwa for helpful discussions.

Supporting Information

Detailed specifications of the GAMMA-CIE model including parameters. Mass transfer coefficient derivation. Additional model output.

References Cited

(1) Weschler, C. J.; Carslaw, N. Indoor Chemistry. *Environ. Sci. Technol.* **2018**, *52* (5), 2419–2428. doi:10.1021/acs.est.7b06387.

(2) Uhde, E.; Salthammer, T. Impact of Reaction Products from Building Materials and Furnishings on Indoor Air Quality-A Review of Recent Advances in Indoor Chemistry. *Atmos. Environ.* **2007**, *41* (15), 3111–3128. doi:10.1016/j.atmosenv.2006.05.082.

(3) Wolkoff, P. Impact of Air Velocity, Temperature, Humidity, and Air on Long-Term VOC Emissions from Building Products. *Atmos. Environ.* **1998**, *32* (14–15), 2659–2668. doi:10.1016/S1352-2310(97)00402-0.

(4) Norback, D.; Wieslander, G.; Nordstrom, K.; Walinder, R. Asthma Symptoms in Relation to Measured Building Dampness in Upper Concrete Floor Construction, and 2-Ethyl-1-Hexanol in Indoor Air. *Int. J. Tuberc. Lung Dis.* **2000**, *4* (11), 1016–1025.

(5) Björk, F.; Eriksson, C. A.; Karlsson, S.; Khabbaz, F. Degradation of Components in Flooring Systems in Humid and Alkaline Environments. *Constr. Build. Mater.* **2003**, *17* (3), 213–221. doi:10.1016/S0950-0618(02)00036-3.

(6) Cano, J. M.; Marín, M. L.; Sánchez, A.; Hernandis, V. Determination of Adipate Plasticizers in Poly(Vinyl Chloride) by Microwave-Assisted Extraction. *J. Chromatogr. A* **2002**, *963* (1–2), 401–409. doi:10.1016/S0021-9673(02)00642-8.

(7) Fromme, H.; Schütze, A.; Lahrz, T.; Kraft, M.; Fembacher, L.; Siewering, S.; Burkardt, R.; Dietrich, S.; Koch, H. M.; Völkel, W. Non-Phthalate Plasticizers in German Daycare Centers and Human Biomonitoring of DINCH Metabolites in Children Attending the

Centers (LUPE 3). *Int. J. Hyg. Environ. Health* **2016**, *219* (1), 33–39. doi:10.1016/j.ijheh.2015.08.002.

(8) Maeng, D. Y.; McNeill, V. F. Kinetics of Alkaline Hydrolysis of Synthetic Organic Esters. *Int. J. Chem. Kinet.* **2022**, *54* (3), 218–222. doi:10.1002/kin.21552.

(9) Wolfe, N. L.; Steen, W. C.; Burns, L. A. Phthalate Ester Hydrolysis: Linear Free Energy Relationships. *Chemosphere* **1980**, *9* (7–8), 403–408. doi:10.1016/0045-6535(80)90023-5.

(10) Shija, R.; Bruce Sunderland, V.; McDonald, C. Alkaline Hydrolysis of Methyl, Ethyl and n-Propyl 4-Hydroxybenzoate Esters in the Liquid and Frozen States. *Int. J. Pharm.* **1992**, *80* (1–3), 203–211. doi:10.1016/0378-5173(92)90278-A.

(11) Bope, A.; Haines, S. R.; Hegarty, B.; Weschler, C. J.; Peccia, J.; Dannemiller, K. C. Degradation of Phthalate Esters in Floor Dust at Elevated Relative Humidity. *Environ. Sci. Process. Impacts* **2019**, *21* (8), 1268–1279. doi:10.1039/c9em00050j.

(12) Wang, L.; Liao, C.; Liu, F.; Wu, Q.; Guo, Y.; Moon, H. B.; Nakata, H.; Kannan, K. Occurrence and Human Exposure of P-Hydroxybenzoic Acid Esters (Parabens), Bisphenol a Diglycidyl Ether (BADGE), and Their Hydrolysis Products in Indoor Dust from the United States and Three East Asian Countries. *Environ. Sci. Technol.* **2012**, *46* (21), 11584–11593. doi:10.1021/es303516u.

(13) McNeill, V. F.; Woo, J. L.; Kim, D. D.; Schwier, A. N.; Wannell, N. J.; Sumner, A. J.; Barakat, J. M. Aqueous-Phase Secondary Organic Aerosol and Organosulfate Formation in Atmospheric Aerosols: A Modeling Study. *Environ. Sci. Technol.* **2012**, *46* (15), 8075–8081. doi:10.1021/es3002986.

(14) Wakayama, T.; Ito, Y.; Sakai, K.; Miyake, M.; Shibata, E.; Ohno, H.; Kamijima, M. Comprehensive Review of 2-Ethyl-1-Hexanol as an Indoor Air Pollutant. *J. Occup. Health* **2019**, *61* (1), 19–35. doi:10.1002/1348-9585.12017.

(15) Lin, C. C.; Corsi, R. L. Texanol® Ester Alcohol Emissions from Latex Paints: Temporal Variations and Multi-Component Recoveries. *Atmos. Environ.* **2007**, *41* (15), 3225–3234. doi:10.1016/j.atmosenv.2006.07.057.

(16) Corsi, R. L.; Lin, C. C. Emissions of 2,2,4-Trimethyl-1,3-Pentanediol Monoisobutyrate (TMPD-MIB) from Latex Paint: A Critical Review. *Crit. Rev. Environ. Sci. Technol.* **2009**, *39* (12), 1052–1080. doi:10.1080/10643380801977925.

(17) Weschler, C. J.; Nazaroff, W. W. Semivolatile Organic Compounds in Indoor Environments. *Atmos. Environ.* **2008**, *42* (40), 9018–9040. doi:10.1016/j.atmosenv.2008.09.052.

(18) Weschler, C. J.; Nazaroff, W. W. Growth of Organic Films on Indoor Surfaces. *Indoor Air* **2017**, *27* (6), 1101–1112. doi:10.1111/ina.12396.

(19) Bergh, C.; Torgrip, R.; Emenius, G.; Östman, C. Organophosphate and Phthalate Esters in Air and Settled Dust - a Multi-Location Indoor Study. *Indoor Air* **2011**, *21* (1), 67–76. doi:10.1111/j.1600-0668.2010.00684.x.

(20) Schwartz, S. E. Mass-Transport Considerations Pertinent to Aqueous Phase Reactions of Gases in Liquid-Water Clouds. In *Chemistry of Multiphase Atmospheric Systems*; Jaeschke, W., Ed.; Springer Berlin Heidelberg: Berlin, Heidelberg, 1986; Vol. 41, pp 415–471. doi:10.1007/978-3-642-70627-1_16.

(21) Shiraiwa, M.; Pfrang, C.; Pöschl, U. Kinetic Multi-Layer Model of Aerosol Surface and Bulk Chemistry (KM-SUB): The Influence of Interfacial Transport and Bulk Diffusion on the Oxidation of Oleic Acid by Ozone. *Atmos. Chem. Phys.* **2010**, *10* (8), 3673–3691. doi:10.5194/acp-10-3673-2010.

(22) Morrison, G.; Lakey, P. S. J.; Abbatt, J.; Shiraiwa, M. Indoor Boundary Layer Chemistry Modeling. *Indoor Air* **2019**, *29* (6), 956–967. doi:10.1111/ina.12601.

(23) Corner, J.; Pendlebury, E. D. The Coagulation and Deposition of a Stirred Aerosol. *Proc. Phys. Soc. Sect. B* **1951**, *64* (8), 645–654. doi:10.1088/0370-1301/64/8/304.

(24) Nazaroff, W. W.; Cass, G. R. Mathematical Modeling of Indoor Aerosol Dynamics. *Environ. Sci. Technol.* **1989**, *23* (2), 157–166. doi:10.1021/es00179a003.

(25) Woo, J. L.; McNeill, V. F. SimpleGAMMA v1.0 - A Reduced Model of Secondary Organic Aerosol Formation in the Aqueous Aerosol Phase (AaSOA). *Geosci. Model Dev.* **2015**, *8* (6), 1821–1829. doi:10.5194/gmd-8-1821-2015.

(26) Staples, C. A.; Peterson, D. R.; Parkerton, T. F.; Adams, W. J. The Environmental Fate of Phthalate Esters: A Literature Review. **1997**, *35* (4), 667–749.

(27) Atkinson, R.; Baulch, D. L.; Cox, R. A.; Crowley, J. N.; Hampson, R. F.; Hynes, R. G.; Jenkin, M. E.; Rossi, M. J.; Troe, J. Evaluated Kinetic and Photochemical Data for Atmospheric Chemistry: Volume II – Gas Phase Reactions of Organic Species. *Atmos. Chem. Phys.* **2006**, *6* (11), 3625–4055. doi:10.5194/acp-6-3625-2006.

(28) US EPA. Estimation Programs Interface Suite™ for Microsoft® Windows, v 4.11. United States Environmental Protection Agency: Washington, DC, USA 2022.

(29) Carslaw, N. A New Detailed Chemical Model for Indoor Air Pollution. *Atmos. Environ.* **2007**, *41* (6), 1164–1179. doi:10.1016/j.atmosenv.2006.09.038.

(30) Weschler, C. J.; Shields, H. C. Production of the Hydroxyl Radical in Indoor Air. *Environ. Sci. Technol.* **1996**, *30* (11), 3250–3258. doi:10.1021/es960032f.

(31) Kirby, A. J. Hydrolysis and Formation of Esters of Organic Acids. In *Comprehensive Chemical Kinetics*; Bamford, C. H., Tipper, C. F. H., Eds.; Elsevier, 1972; Vol. 10, pp 57–207. doi:10.1016/S0069-8040(08)70344-3.

(32) Su, G.; Letcher, R. J.; Yu, H. Organophosphate Flame Retardants and Plasticizers in Aqueous Solution: PH-Dependent Hydrolysis, Kinetics, and Pathways. *Environ. Sci. Technol.* **2016**, *50* (15), 8103–8111. doi:10.1021/acs.est.6b02187.

(33) Björk, F.; Eriksson, C. A. Measurement of Alkalinity in Concrete by a Simple Procedure, to Investigate Transport of Alkaline Material from the Concrete Slab to a Self-Levelling Screed. *Constr. Build. Mater.* **2002**, *16* (8), 535–542. doi:10.1016/S0950-0618(02)00035-1.

(34) Räsänen, V.; Penttala, V. The PH Measurement of Concrete and Smoothing Mortar Using a Concrete Powder Suspension. *Cem. Concr. Res.* **2004**, *34* (5), 813–820. doi:10.1016/j.cemconres.2003.09.017.

(35) Howard-Reed, C.; Wallace, L. A.; Ott, W. R. The Effect of Opening Windows on Air Change Rates in Two Homes. *J. Air Waste Manag. Assoc.* **2002**, *52* (2), 147–159. doi:10.1080/10473289.2002.10470775.

(36) McNeill, V. F.; Corsi, R.; Huffman, J. A.; King, C.; Klein, R.; Lamore, M.; Maeng, D. Y.;

Miller, S. L.; Lee Ng, N.; Olsiewski, P.; Godri Pollitt, K. J.; Segalman, R.; Sessions, A.; Squires, T.; Westgate, S. Room-Level Ventilation in Schools and Universities. *Atmos. Environ. X* **2022**, *13*, 100152. doi:10.1016/j.aeaoa.2022.100152.

(37) Daghigh, R.; Adam, N. M.; Sahari, B. B. Ventilation Parameters and Thermal Comfort of Naturally and Mechanically Ventilated Offices. *Indoor Built Environ.* **2009**, *18* (2), 113–122. doi:10.1177/1420326X09103013.

(38) Letinski, D. J.; Connelly, M. J.; Peterson, D. R.; Parkerton, T. F. Slow-Stir Water Solubility Measurements of Selected Alcohols and Diesters. *Chemosphere* **2002**, *48* (3), 257–265. doi:10.1016/S0045-6535(02)00086-3.

(39) Russell, D. J.; McDuffie, B. Chemodynamic Properties of Phthalate Esters: Partitioning and Soil Migration. *Chemosphere* **1986**, *15* (8), 1003–1021. doi:10.1016/0045-6535(86)90553-9.

(40) Lakey, P. S. J.; Eichler, C. M. A.; Wang, C.; Little, J. C.; Shiraiwa, M. Kinetic Multi-Layer Model of Film Formation, Growth, and Chemistry (KM-FILM): Boundary Layer Processes, Multi-Layer Adsorption, Bulk Diffusion, and Heterogeneous Reactions. *Indoor Air* **2021**, *31* (6), 2070–2083. doi:10.1111/ina.12854.

(41) Schwartz-Narbonne, H.; Donaldson, D. J. Water Uptake by Indoor Surface Films. *Sci. Rep.* **2019**, *9* (1), 11089. doi:10.1038/s41598-019-47590-x.

(42) Duncan, S. M.; Sexton, K. G.; Turpin, B. J. Oxygenated VOCs, Aqueous Chemistry, and Potential Impacts on Residential Indoor Air Composition. *Indoor Air* **2018**, *28* (1), 198–212. doi:10.1111/ina.12422.

(43) Sollinger, S.; Levsen, K.; Wünsch, G. Indoor Pollution by Organic Emissions from Textile Floor Coverings: Climate Test Chamber Studies under Static Conditions. *Atmos. Environ.* **1994**, *28* (14), 2369–2378. doi:10.1016/1352-2310(94)90491-X.

(44) Manuja, A.; Ritchie, J.; Buch, K.; Wu, Y.; Eichler, C. M. A.; Little, J. C.; Marr, L. C. Total Surface Area in Indoor Environments. *Environ. Sci. Process. Impacts* **2019**, *21* (8), 1384–1392. doi:10.1039/c9em00157c.

(45) Fromme, H.; Lahrz, T.; Piloty, M.; Gebhart, H.; Oddoy, A.; Rüden, H. Occurrence of Phthalates and Musk Fragrances in Indoor Air and Dust from Apartments and Kindergartens in Berlin (Germany). *Indoor Air* **2004**, *14* (3), 188–195. doi:10.1111/j.1600-0668.2004.00223.x.

(46) Norbäck, D.; Wieslander, G.; Edling, C. Occupational Exposure to Volatile Organic Compounds (VOCS), and Other Air Pollutants from the Indoor Application of Water-Based Paints. *Ann. Occup. Hyg.* **1995**, *39* (6), 783–794. doi:10.1093/annhyg/39.6.783.

(47) Gallego, E.; Roca, X.; Perales, J. F.; Guardino, X. Determining Indoor Air Quality and Identifying the Origin of Odour Episodes in Indoor Environments. *J. Environ. Sci.* **2009**, *21* (3), 333–339. doi:10.1016/S1001-0742(08)62273-1.

(48) Brown, S. K.; Sim, M. R.; Abramson, M. J.; Gray, C. N. Concentrations of Volatile Organic Compounds in Indoor Air – A Review. *Indoor Air* **1994**, *4* (2), 123–134. doi:10.1111/j.1600-0668.1994.t01-2-00007.x.

(49) Gerster, F. M.; Hopf, N. B.; Wild, P. P.; Vernez, D. Airborne Exposures to Monoethanolamine, Glycol Ethers, and Benzyl Alcohol during Professional Cleaning: A

Pilot Study. *Ann. Occup. Hyg.* **2014**, *58* (7), 846–859. doi:10.1093/annhyg/meu028.

(50) Sander, R. Modeling Atmospheric Chemistry: Interactions between Gas-Phase Species and Liquid Cloud/Aerosol Particles. *Surv. Geophys.* **1999**, *20* (1), 1–31. doi:10.1023/A:1006501706704.

(51) Sander, R. Compilation of Henry's Law Constants (Version 4.0) for Water as Solvent. *Atmos. Chem. Phys.* **2015**, *15* (8), 4399–4981. doi:10.5194/acp-15-4399-2015.

(52) Tilgner, A.; Schaefer, T.; Alexander, B.; Barth, M.; Collett, J. L.; Fahey, K. M.; Nenes, A.; Pye, H. O. T.; Herrmann, H.; McNeill, V. F. Acidity and the Multiphase Chemistry of Atmospheric Aqueous Particles and Clouds. *Atmos. Chem. Phys.* **2021**, *21* (17), 13483–13536. doi:10.5194/acp-21-13483-2021.

(53) Nalli, S.; Horn, O. J.; Grochowalski, A. R.; Cooper, D. G.; Nicell, J. A. Origin of 2-Ethylhexanol as a VOC. *Environ. Pollut.* **2006**, *140* (1), 181–185. doi:10.1016/j.envpol.2005.06.018.

(54) Wei, Z.; Li, Y.; Cooks, R. G.; Yan, X. Accelerated Reaction Kinetics in Microdroplets: Overview and Recent Developments. *Annu. Rev. Phys. Chem.* **2020**, *71*, 31–51. doi:10.1146/annurev-physchem-121319-110654.

(55) Banerjee, S.; Gnanamani, E.; Yan, X.; Zare, R. N. Can All Bulk-Phase Reactions Be Accelerated in Microdroplets? *Analyst* **2017**, *142* (9), 1399–1402. doi:10.1039/c6an02225a.

(56) Sjöberg, A.; Ramnäs, O. An Experimental Parametric Study of VOC from Flooring Systems Exposed to Alkaline Solutions. *Indoor Air* **2007**, *17* (6), 450–457. doi:10.1111/j.1600-0668.2007.00492.x.

(57) Chino, S.; Kato, S.; Seo, J.; Ataka, Y. Study on Emission of Decomposed Chemicals of Esters Contained in PVC Flooring and Adhesive. *Build. Environ.* **2009**, *44* (7), 1337–1342. doi:10.1016/j.buildenv.2008.07.003.

(58) Sparks, L. E.; Guo, Z.; Chang, J. C.; Tichenor, B. A. Volatile Organic Compound Emissions from Latex Paint - Part 2. Test House Studies and Indoor Air Quality (IAQ) Modeling. *Indoor Air* **1999**, *9* (1), 18–25. doi:10.1111/j.1600-0668.1999.t01-3-00004.x.

(59) Chang, J. C. S.; Tichenor, B. A.; Guo, Z.; Krebs, K. A. Substrate Effects on VOC Emissions from a Latex Paint. *Indoor Air* **1997**, *7* (4), 241–247. doi:10.1111/j.1600-0668.1997.00003.x.

(60) South Coast Air Quality Management District. *Final Program Environmental Impact Report for the 2012 Air Quality Management Plan*; 2012.

(61) Jones, A. P. Indoor Air Quality and Health. *Atmos. Environ.* **1999**, *33* (28), 4535–4564. doi:10.1016/S1352-2310(99)00272-1.

(62) Salthammer, T.; Fuhrmann, F.; Uhde, E. Flame Retardants in the Indoor Environment - Part II: Release of VOCs (Triethylphosphate and Halogenated Degradation Products) from Polyurethane. *Indoor Air* **2003**, *13* (1), 49–52. doi:10.1034/j.1600-0668.2003.01150.x.

(63) Lam, B.; Diamond, M. L.; Simpson, A. J.; Makar, P. A.; Truong, J.; Hernandez-Martinez, N. A. Chemical Composition of Surface Films on Glass Windows and Implications for Atmospheric Chemistry. *Atmos. Environ.* **2005**, *39* (35), 6578–6586. doi:10.1016/j.atmosenv.2005.07.057.

(64) Nazaroff, W. W.; Weschler, C. J. Indoor Acids and Bases. *Indoor Air* **2020**, No. March,

559–644. doi:10.1111/ina.12670.

(65) Jencks, W. P.; Carriuolo, J. General Base Catalysis of Ester Hydrolysis. *J. Am. Chem. Soc.* **1961**, *83* (7), 1743–1750. doi:10.1021/ja01468a044.

(66) Fersht, A. R.; Kirby, A. J. The Hydrolysis of Aspirin. Intramolecular General Base Catalysis of Ester Hydrolysis. *J. Am. Chem. Soc.* **1967**, *89* (19), 4857–4863. doi:10.1021/ja00995a007.

(67) Stefanidis, D.; Jencks, W. P. General Base Catalysis of Ester Hydrolysis. *J. Am. Chem. Soc.* **1993**, *115* (14), 6045–6050. doi:10.1021/ja00067a020.

(68) Ault, A. General Acid and General Base Catalysis. *J. Chem. Educ.* **2007**, *84* (1), 38–39. doi:10.1021/ed084p38.

(69) Ault, A. P.; Grassian, V. H.; Carslaw, N.; Collins, D. B.; Destaillats, H.; Donaldson, D. J.; Farmer, D. K.; Jimenez, J. L.; McNeill, V. F.; Morrison, G. C.; O'Brien, R. E.; Shiraiwa, M.; Vance, M E.; Wells, J. R.; Xiong, W. Indoor Surface Chemistry: Developing a Molecular Picture of Reactions on Indoor Interfaces. *Chem* **2020**, 1–16. doi:10.1016/j.chempr.2020.08.023.

Supporting Information for "Numerical Simulations of Synthetic Ester Hydrolysis in the Indoor Environment"

Do Young Maeng[1] *and V. Faye McNeill*[1,2]*

[1]Department of Chemical Engineering, Columbia University, New York, NY USA 10027

[2]Department of Earth and Environmental Sciences, Columbia University, New York, NY USA 10027

* to whom correspondence should be addressed. vfm2103@columbia.edu

Summary: 25 pages, 6 figures, 12 tables

Table of Contents

Model Specification

Table S1. List of chemical species

Name	Abbreviation	Phase
Hydroxyl radical	OH	gas
Hydroxide ion	OH^-	Aq
Bis(2-ethylhexyl) adipate	DEHA	gas, aq
Bis(2-ethylhexyl) phthalate	DEHP	gas, aq
Mono(2-ethylhexyl) adipate	MEHA	gas, aq
Mono(2-ethylhexyl) phthalate	MEHP	gas, aq
2-Ethylhexanol	2-EH	gas, aq
2,2,4-Trimethyl-1,3-pentanediol monoisobutyrate	TMPD-MIB	gas, aq
Isobutyric acid	IBA	gas, aq
2,2,4-Trimethyl-1,3-pentanediol	TMPD	gas, aq
Diethyl phthalate	DEP	gas, aq
Diisobutyl phthalate	DIBP	gas, aq
Dibutyl phthalate	DBP	gas, aq
Butyl benzyl phthalate	BBzP	gas, aq
Tris(2-chloroethyl) phosphate	TCEP	gas, aq
Tris(1-chloro-2-propyl) phosphate	TCIPP	gas, aq
Monoethyl phthalate	MEP	gas, aq
Monoisobutyl phthalate	MIBP	gas, aq
Monobutyl phthalate	MBP	gas, aq
Monobenzyl phthalate	MBzP	gas, aq
Bis(2-chloroethyl) phosphate	BCEP	gas, aq

Bis(1-chloro-2-propyl) phosphate	BCIPP	gas, aq
Phthalic acid	PA	gas, aq
Ethanol	EtOH	gas, aq
Isobutanol	*i*-BuOH	gas, aq
Butanol	BuOH	gas, aq
Benzyl alcohol	BnOH	gas, aq
2-chloroethanol	2-CE	gas, aq
1-chloro-2-propanol	1C2P	gas, aq

Table S2. List of Henry's law constants at 25 °C

Species	**H (M/atm)**	**Reference**
DEHA	2.30E+03	(1)
DEHP	22.9	(2)
MEHA	1E+05[a]	(3)
MEHP	5E+05[a]	(3)
2-EH	69.62	(4)
TMPD-MIB	1E+04[a]	(3)
IBA	1E+03	(5)
TMPD	1.4E+03	(5)
DEP	1.64E+03	(2)
DIBP	820	(2)
DBP	552	(2)
BBzP	1E+04	(5)
TCEP	3E+02	(5)
TCIPP	1.6E+02	(5)
MEP	2E+06[a]	(3)
MIBP	1E+06[a]	(3)
MBP	1E+06[a]	(3)
MBzP	1E+08[a]	(3)
BCEP	6E+06[a]	(3)

BCIPP	3E+06[a]	(3)
PA	5E+07	(5)
AA	2E+08	(5)
EtOH	2E+02	(5)
i-BuOH	1E+02	(5)
BuOH	1.2E+02	(5)
BnOH	2.9E+03	(5)
2-CE	9.6E+03	(5)
1C2P	5.7E+02	(5)

[a]Estimation from EPI Suite HENRYWIN

Table S3. Gas-phase oxidation kinetics

Reaction	kOH (cm^3 $molec^{-1}$ s^{-1})	T (°C)	Reference
DEHA + OH → OXIDATION PRODUCTS	2.5E-11[a]	25	(3)
MEHA + OH → OXIDATION PRODUCTS	1.5E-11[a]	25	(3)
DEHP + OH → OXIDATION PRODUCTS	2.2E-11[a]	25	(3)
MEHP + OH → OXIDATION PRODUCTS	1.2E-11[a]	25	(3)
DEP + OH → OXIDATION PRODUCTS	3.5E-12[a]	25	(3)
MEP + OH → OXIDATION PRODUCTS	2.4E-12[a]	25	(3)
DBP + OH → OXIDATION PRODUCTS	9.3E-12[a]	25	(3)
MBP + OH → OXIDATION PRODUCTS	5.3E-12[a]	25	(3)
DIBP + OH → OXIDATION PRODUCTS	9.3E-12[a]	25	(3)
MIBP + OH → OXIDATION PRODUCTS	5.3E-12[a]	25	(3)
TCIPP + OH → OXIDATION PRODUCTS	4E-11[a]	25	(3)
TCEP + OH → OXIDATION PRODUCTS	2E-11[a]	25	(3)
BBzP + OH → OXIDATION PRODUCTS	1.1E-11[a]	25	(3)
MBzP + OH → OXIDATION PRODUCTS	7E-12[a]	25	(3)
TMPD-MIB + OH → OXIDATION PRODUCTS	1.6E-11[a]	25	(3)
BCIPP + OH → OXIDATION PRODUCTS	3E-11[a]	25	(3)
BCEP + OH → OXIDATION PRODUCTS	1.5E-11[a]	25	(3)
IBA + OH → OXIDATION PRODUCTS	2E-12[a]	25	(3)
PA + OH → OXIDATION PRODUCTS	1E-12[a]	25	(3)
EtOH + OH → OXIDATION PRODUCTS	3.2E-12	25	(6)
BuOH + OH → OXIDATION PRODUCTS	8.5E-12	25	(6)
i-BuOH + OH → OXIDATION PRODUCTS	7E-12[a]	25	(3)
BnOH + OH → OXIDATION PRODUCTS	2.7E-11	25	(6)
2-EH + OH → OXIDATION PRODUCTS	1.13E-11	25	(7)
TMPD + OH → OXIDATION PRODUCTS	2E-11[a]	25	(3)
2-CE + OH → OXIDATION PRODUCTS	1.8E-12[a]	25	(3)
1C2P + OH → OXIDATION PRODUCTS	3.2E-12[a]	25	(3)

[a]Estimation from EPI Suite AOPWIN

Table S4. Aqueous-phase hydrolysis kinetics

Reaction	kOH^- (M^{-1} s^{-1})	T (°C)	Reference
DEHA + OH^- → MEHA + 2-EH	4.8E-04	21	(8)
MEHA + OH^- → 2-EH + ADIPIC ACID	3E-02[a]	25	(3)
DEHP + OH^- → MEHP + 2-EH	1.1E-04	30	(9)
MEHP + OH^- → 2-EH + PA	2E-02[a]	25	(3)
DEP + OH^- → MEP + EtOH	2.5E-02	30	(9)
MEP + OH^- → EtOH + PA	4E-02[a]	25	(3)
DBP + OH^- → MNBP + BuOH	1.0E-02	30	(9)
MBP + OH^- → BuOH + PA	3E-02[a]	25	(3)
DIBP + OH^- → MIBP + *i*-BuOH	1.4E-03	30	(9)
MIBP + OH^- → *i*-BuOH + PA	2E-02[a]	25	(3)
TCIPP + OH^- → BCIPP + 1C2P	7.2E-06	20	(10)
TCEP + OH^- → BCEP + 2-CE	9.7E-04	20	(10)
BBzP + OH^- → MBzP + BnOH	5.9E-02	21	(8)
MBzP + OH^- → BnOH + PA	1E-01[a]	25	(3)
TMPD-MIB + OH^- →TMPD + IBA	9.8E-03	20	(8)

[a]Estimation from EPI Suite HYDROWIN

Table S5. Initial conditions, hydrolysis of DEHA and DEHP

Species	Concentration (M)	Notes	Reference
DEHA (aq)	8.6E-09	DEHA water solubility. Held constant throughout simulation.	(11)
DEHP (aq) (low)	4.9E-09	DEHP water solubility. Held constant throughout simulation. For low-DEHP condition	(11)
DEHP (aq) (high)	1E-06	DEHP water solubility. Held constant throughout simulation. For high-DEHP condition	(11)

Table S6. Initial conditions, hydrolysis of TMPD-MIB

Species	Concentration (M)	Notes	Reference
TMPD-MIB (aq)	4E-02	Calculated on the basis of mass composition and bulk density of latex paint (0.67% mass)	(12)

Table S7. Initial conditions, hydrolysis of common PEs and PFRs

Species	Concentration (ng/m^3)	Notes	Reference
DEP (g)	1598	Mean measurement at homes in Sweden. Held constant throughout simulation	(13)
DIBP (g)	310	Mean measurement at workplaces in Sweden. Held constant throughout simulation	(13)
DBP (g)	925	Mean measurement at homes in Sweden. Held constant throughout simulation	(13)
BBzP (g)	28	Mean measurement at homes in Sweden. Held constant throughout simulation	(13)
TCEP (g)	47	Mean measurement at day care centers in Sweden. Held constant throughout simulation	(13)
TCIPP (g)	110	Mean measurement at workplaces in Sweden. Held constant throughout simulation	(13)

Table S8. List of pKa

Species	pKa1	pKa2	T (°C)	Reference
IBA	4.84	*N/A*	20	(14)
PA	2.76	4.92	25	(15)
AA	4.44	5.44	25	(15)

Boundary Layer Characterization

In GAMMA-CIE, the boundary layer consists of 26 layers with varying thickness: 1.8E-1 cm for layers 1 (topmost) to 5; 1.8E-2 cm for layers 6 to 10; 1.8E-3 cm for layers 11 to 15; 1.8E-4 cm for layers 16 to 20; 1.8E-5 cm for layers 21 to 25; and 1E-5 cm for layer 26. Figure S1 below illustrates the evolution of 2-EH in Scenario 1 for different layers. The layers near the aqueous film are of thinner thickness to characterize the initial, rapid transport of gas species near the surface following their production in the aqueous film. As expected for species that are not highly reactive to atmospheric oxidation, the concentration differences among layers in the boundary layer are minimal, and the bulk air concentration is several orders of magnitude lower due to the greater dilution factor and loss by ventilation in this layer.

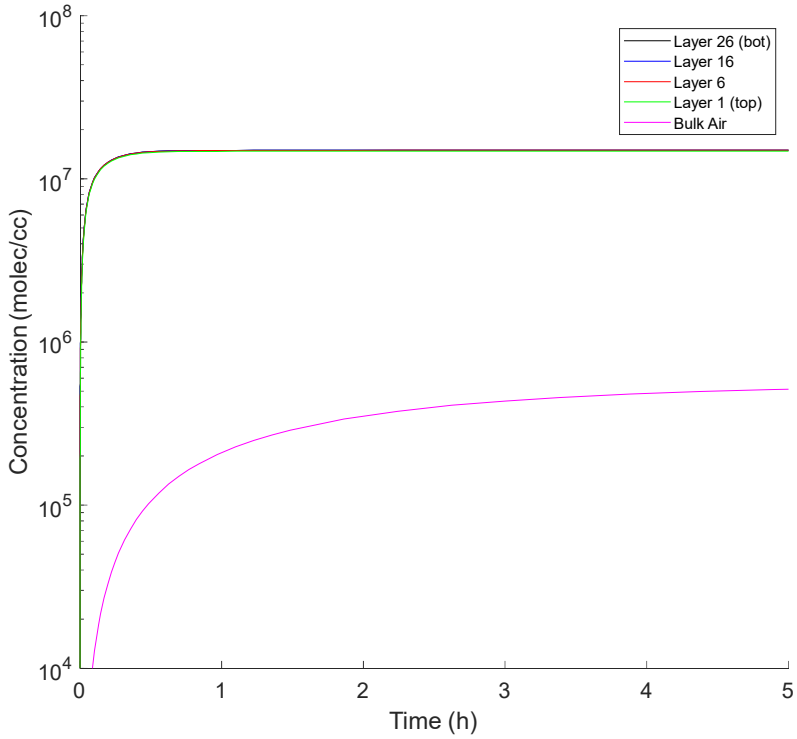

Figure S1. 2-EH concentration profile in various gas-phase layers for Scenario 1 at pH 13 and 0.5 ACH

Gas-Phase Molecular Diffusion Coefficient Estimation

The gas-phase molecular diffusion coefficient estimation is as follows (16):

$$D_{m,i} = 1.9(\mathrm{MW})^{-2/3}$$

where $D_{m,i}$ is the gas-phase molecular diffusion coefficient ($cm^2\ s^{-1}$) and MW is the molecular weight ($g\ mol^{-1}$).

Mass Transfer Coefficient Derivation

Closely following Schwartz (1986) (17), the mass transfer coefficient considers: (1) gas-phase diffusion of species *i* into the film and (2) interphase mass transport but has been modified to consider transport for a planar film instead of a spherical aerosol particle.

Gas-phase diffusion

We start with the gas-phase diffusion of species *i* in the bottommost layer (i.e., *n*th layer) of the boundary layer (BL) into the film in the absence of reactions, resulting in the following equation:

$$\frac{\partial C_g}{\partial t} - D_g \frac{\partial^2 C_g}{\partial y^2} = 0$$

where C_g is the gas-phase concentration of species i, t is time, and y is distance normal to the film surface. We assume the following conditions at which the flux into the film is maximized: (1) steady-state conditions, (2) $C_g = 0$ at $y = 0$ (at the film surface), and (3) $C_g = C_{g,eq}$ at $y = \delta_n$, where δ_n is the thickness of the bottommost BL layer. Additionally, we also assume the bottommost layer in BL is quiescent (i.e., eddy diffusion is not considered), resulting in the equation below for the gas-phase concentration, C_g:

$$C_g = \frac{C_{g,eq}}{\delta_n} y$$

The maximum steady-state flux of species *i, $F_{max,g}$,* is:

$$F_{max,g} = -D_g \frac{dC_g}{dy} = -D_g \frac{C_{g,eq}}{\delta_n}$$

Using the expression above, we define the average molar uptake rate of species *i, $R_{max,g}$,* into the aqueous planar film and express it in partial pressure of species *i* at equilibrium, P_{eq}:

$$R_{max,g} = -\frac{A_{film}}{V_{film}} F = \frac{D_g C_{g,eq}}{\delta_{film}\delta_n} = \frac{D_g P_{eq}}{\delta_{film}\delta_n \mathrm{R}T}$$

where δ_{film} is the thickness of the aqueous film, R is the gas constant, and T is temperature. The time constant of film saturation of species *i* by gas-phase diffusion, τ_g, is in the order of $\delta_{film}\delta_n/D_g$ as shown below:

$$\tau_g = \frac{C_{aq,eq}}{R_{max,g}} = \frac{H^* RT \delta_{film}\delta_n}{D_g} \approx \frac{\delta_{film}\delta_n}{D_g}$$

Interphase mass transport

The interphase mass transport expression is on the basis of molecular collision of gas-phase species i on the aqueous-phase surface and is as follows:

$$\sigma_{coll} = \frac{P_{eq}\omega_i \alpha_i}{4\mathrm{R}T}$$

where ω_i is the thermal velocity of species *i* and α_i is the accommodation coefficient of species *i*. The partial pressure of species i should be its value at the interface ($y = 0$), but it is assumed here to be its value at equilibrium to determine the maximum average molar uptake rate, $R_{max,i}$, which is shown below:

$$R_{max,i} = -\frac{A_{film}}{V_{film}} \sigma_{coll} = \frac{P_{eq}\omega_i \alpha_i}{4\delta_{film}\mathrm{R}T}$$

The time constant of film saturation of species *i* by interphase mass transport, τ_i, is in the order of $4\delta_{film}/(\omega_i\alpha_i)$ as shown in the following equation:

$$\tau_i = \frac{C_{aq,eq}}{R_{max,i}} = \frac{4\delta_{film}H^*\mathrm{R}T}{\omega_i\alpha_i} \approx \frac{4\delta_{film}}{\omega_i\alpha_i}$$

Mass transfer coefficient

The mass transfer coefficient considers the time constants (i.e., resistances) of both gas-phase diffusion and interphase mass transport:

$$k_{mt} = (\tau_g + \tau_i)^{-1}$$

$$k_{mt} = \left(\frac{\delta_{film}\delta_n}{D_g} + \frac{4\delta_{film}}{\omega_i\alpha_i}\right)^{-1}$$

Effective Henry's Law Constant

The equations for the effective Henry's law constant are given in Tilgner et al. (2021) (18):

$$H_A{}^* = H_A\left(1 + \frac{K_{a1}}{[\mathrm{H}^+]}\right) \qquad \text{for monoprotic acid}$$

$$H_A{}^* = H_A\left(1 + \frac{K_{a1}}{[\mathrm{H}^+]} + \frac{K_{a1}K_{a2}}{[\mathrm{H}^+]^2}\right) \qquad \text{for diprotic acid}$$

where $H_A{}^*$ is the effective Henry's law constant, H_A is the Henry's law constant, $[H^+]$ is the hydrogen ion concentration, and Ka1 and Ka2 are the acid dissociation constants. Using the HA and pKa values in Tables S2 and S8, the effective Henry's law constant for IBA, PA, and AA are calculated below at pH 10 and 13.

Table S9. List of effective Henry's law constant for acids

Species	H_A (M/atm)	$H_A{}^*$ at pH 10 (M/atm)	$H_A{}^*$ at pH 13 (M/atm)	T (°C)
IBA	1E+03	1.4E+08	1.4E+11	20
PA	5E+07	1.0E+20	1.0E+26	25
AA	2E+08	2.6E+18	2.6E+24	25

Timescale of Loss by Ventilation vs. Atmospheric Oxidation by OH Radical

The following equations describe the timescales of two gas-phase processes, loss by ventilation and loss by atmospheric oxidation by OH radical:

$$\tau_{vent} = \frac{1}{ACH}$$

$$\tau_{ox} = \frac{1}{k_{ox} C_{\cdot OH}}$$

where τ_{vent} is the timescale of ventilation, ACH is the air changes per hour (converted to air changes per second), τ_{ox} is the timescale of atmospheric oxidation, k_{ox} is the second-order oxidation rate constant, and $C_{\cdot OH}$ is the OH radical concentration indoors.

At 0.5 ACH, the timescale associated with loss by ventilation is 7200 s.

$$\tau_{vent} = \frac{1}{0.5\ \mathrm{h}^{-1}} = 2\ \mathrm{h} = 7200\ \mathrm{s}$$

Assuming OH radical concentration of 4×10^5 molec cm^{-3} and k_{ox} of 4×10^{-11} cm^3 molec^{-1} s^{-1} for TCIPP (fastest gas-phase oxidation rate constant in GAMMA-CIE, found in Table S3), the timescale associated with loss by atmospheric oxidation is 62500 s, greater by a factor of 8.7 than that associated with ventilation.

$$\tau_{ox} = \frac{1}{k_{ox} C_{\cdot OH}} = \frac{1}{(4 \times 10^5)(4 \times 10^{-1}\ )\ \mathrm{s}^{-1}} = 62500\ s$$

Scenario 1 Model Output

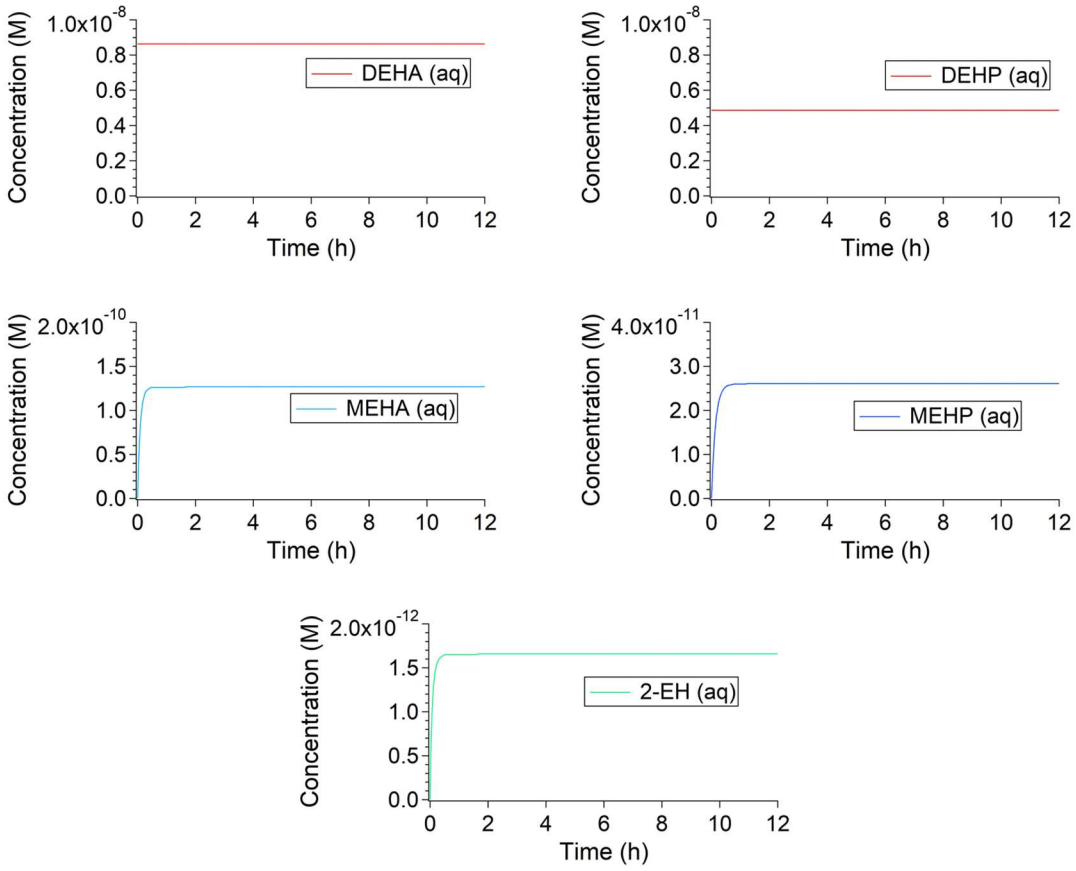

Figure S2. Predicted temporal evolution of aqueous-phase DEHA, DEHP, MEHA, MEHP, and 2-EH at pH 13 and 0.5 ACH in low-DEHP scenario.

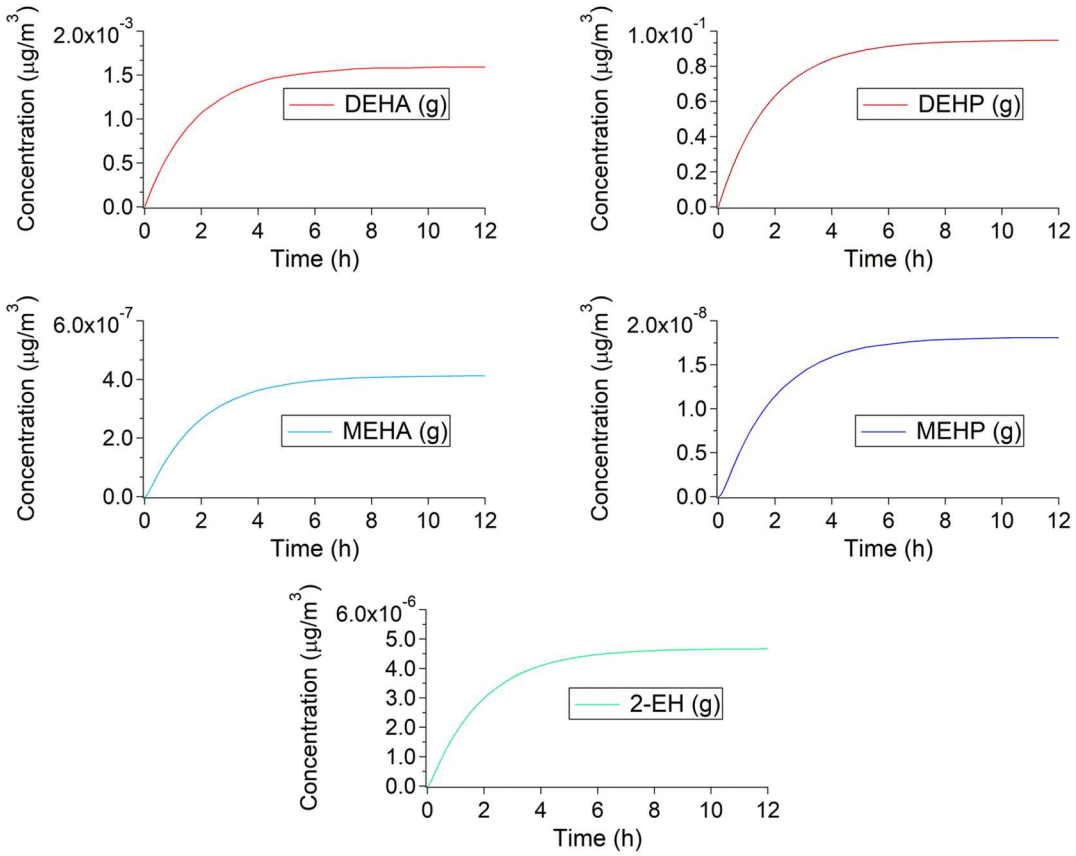

Figure S3. Predicted temporal evolution of gas-phase DEHA, DEHP, MEHA, MEHP, and 2-EH at pH 13 and 0.5 ACH in low-DEHP scenario.

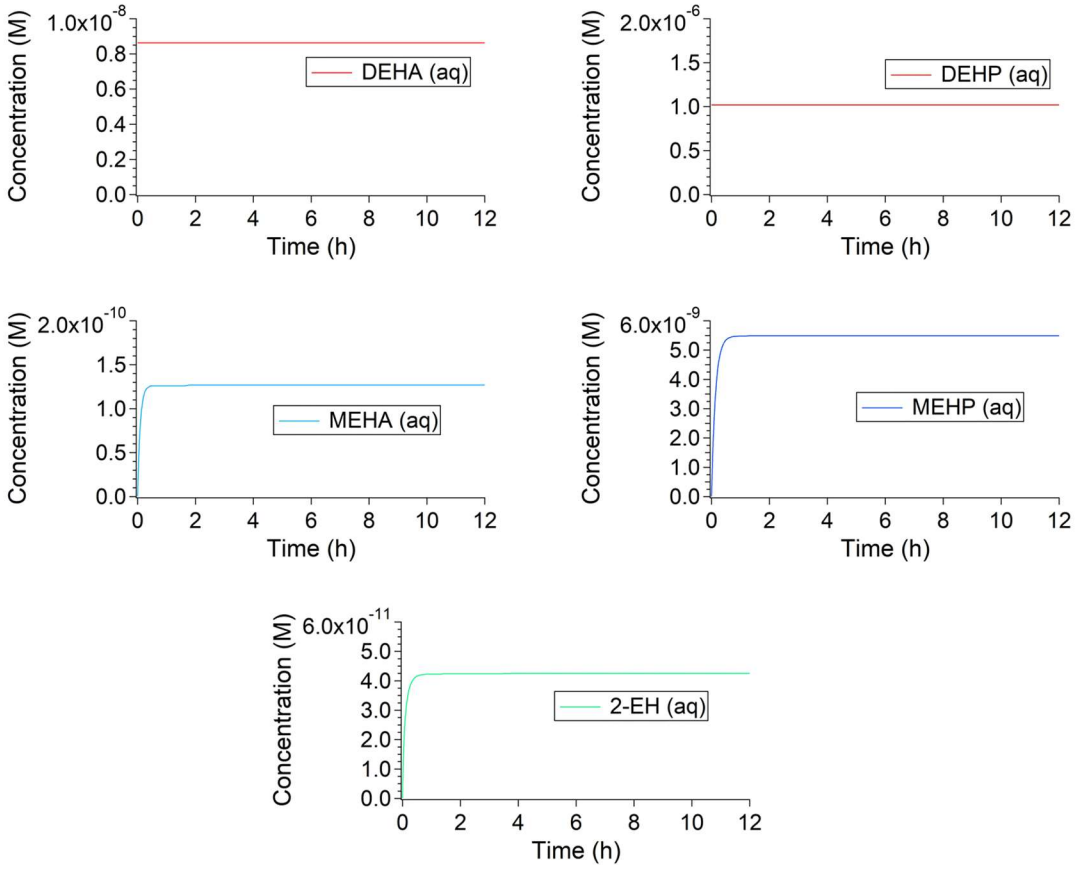

Figure S4. Predicted temporal evolution of aqueous-phase DEHA, DEHP, MEHA, MEHP, and 2-EH at pH 13 and 0.5 ACH in high-DEHP scenario.

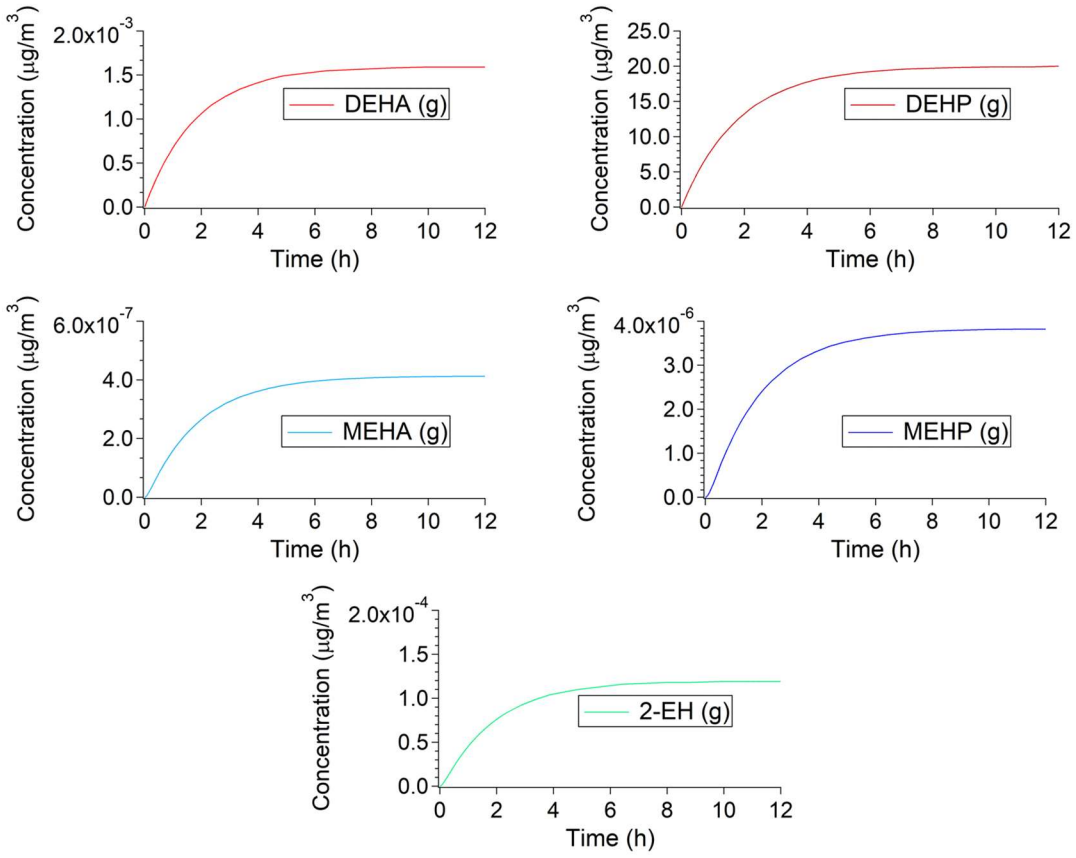

Figure S5. Predicted temporal evolution of gas-phase DEHA, DEHP, MEHA, MEHP, and 2-EH at pH 13 and 0.5 ACH in high-DEHP scenario**.**

Film Thickness Sensitivity Analysis

Film thickness was varied from 1 nm to 100 µm for the simulation of gas-phase 2-ethylhexanol (2-EH) generation in Scenario 1, pH 13, 0.5 ACH, high-DEHP condition to test the sensitivity of the system to film thickness. Figure S6 shows the 2-EH concentration profiles with varying thickness, with the predicted steady state concentrations are tabulated in Table S8 below.

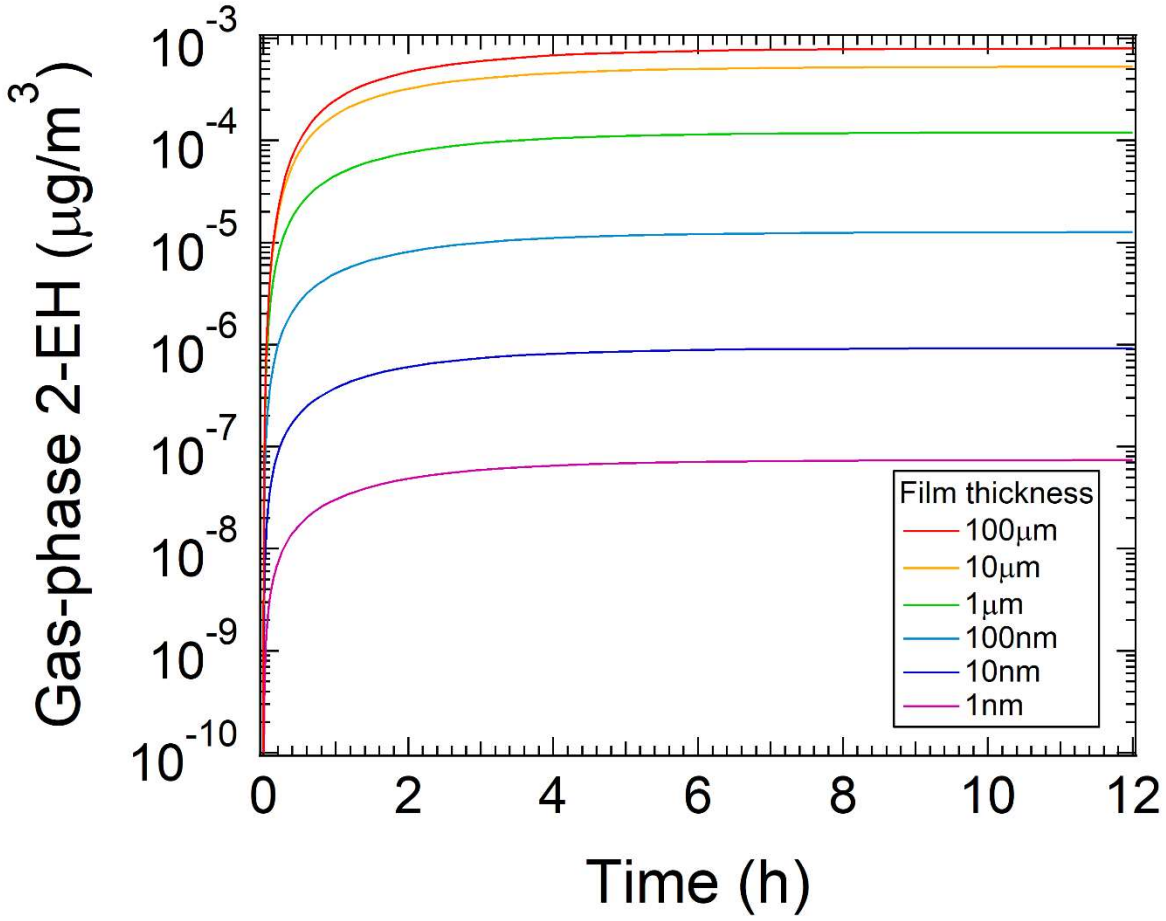

Figure S6. Scenario 1: sensitivity of temporal evolution of gas-phase 2-EH at pH 13 and 0.5 ACH in high-DEHP condition to aqueous film thickness**.**

Table S10. Scenario 1: predicted steady state 2-EH concentrations at pH 13, 0.5 ACH, high-DEHP condition, and varying aqueous film thickness

Aqueous Film Thickness	2-EH Concentration (μg/m^3)
100 μm	7.9E-04
10 μm	5.3E-04
1 μm	1.2E-04
100 nm	1.3E-05
10 nm	9.2E-07
1 nm	7.4E-08

Overall, the predicted steady state concentration decreased with decreasing film thickness. This was expected, with one of the key assumptions in Scenario 1 being that the parent reactant esters DEHA and DEHP would be in excess and remain at aqueous saturation limit throughout the simulation. Thus, thinner aqueous films would indicate lower amount of DEHA and DEHP available in the system. In the lower range of film thickness from 1 nm to 1 μm, a tenfold decrease in film thickness corresponded to approximately a proportional tenfold decrease in the predicted gas-phase 2-EH concentration at steady state. In the higher range from 1 μm to 100 μm, however, changes in film thickness were not as impactful in the evolution of gas-phase 2-EH, with only an eightfold increase in 2-EH concentration corresponding to a hundredfold increase in film thickness. A similar trend between film thickness and gas-phase evolution was observed in both Scenario 2 and 3 as shown in Table S9 and S10 below.

Table S11. Scenario 2: predicted peak TMPD-MIB concentrations at pH 10, 0.5 ACH, and varying aqueous film thickness

Aqueous Film Thickness	2-EH Concentration (μg/m^3)
100 μm	810
10 μm	726
1 μm	356
100 nm	61
10 nm	6.6

1 nm	0.67

Table S12. Scenario 3: predicted steady state EtOH concentrations at pH 13, 0.5 ACH, and varying aqueous film thickness

Aqueous Film Thickness	2-EH Concentration (μg/m^3)
100 μm	9.3E-03
10 μm	4.8E-03
1 μm	3.7E-04
100 nm	9.8E-06
10 nm	5.0E-07
1 nm	3.3E-08

The simulation results suggest that film thickness can significantly affect the gas-phase evolution of hydrolysis products, especially in the 1 nm–1 μm range which is believed to be the likely scale for indoor film thickness (19). In the model, film thickness restricts the overall load of synthetic esters (SEs) available for hydrolytic degradation and gas-phase partitioning in the aqueous film, as the SEs are bound by their water solubilities. The predicted trend may not hold true in practice if SE concentrations can exceed water solubility limits in presence of other organics in the film. Further research is needed to fully understand the impact of film thickness on the emissions of hydrolysis products.

References

1. Felder JD, Adams WJ, Saeger VW. Assessment of the safety of dioctyl adipate in freshwater environments. Environ Toxicol Chem [Internet]. 1986 Aug;5(8):777–84. Available from: https://onlinelibrary.wiley.com/doi/10.1002/etc.5620050809

2. Magdouli S, Daghrir R, Brar SK, Drogui P, Tyagi RD. Di 2-ethylhexylphtalate in the aquatic and terrestrial environment: A critical review. J Environ Manage [Internet]. 2013;127:36–49. Available from: http://dx.doi.org/10.1016/j.jenvman.2013.04.013

3. US EPA. Estimation Programs Interface Suite™ for Microsoft® Windows, v 4.11. Washington, DC, USA: United States Environmental Protection Agency; 2022.

4. Hiatt MH. Determination of Henry's law constants using internal standards with benchmark values. J Chem Eng Data. 2013;58(4):902–8.

5. Sander R. Compilation of Henry's law constants (version 4.0) for water as solvent. Atmos Chem Phys. 2015;15(8):4399–981.

6. Atkinson R, Baulch DL, Cox RA, Crowley JN, Hampson RF, Hynes RG, et al. Evaluated kinetic and photochemical data for atmospheric chemistry: Volume II – gas phase reactions of organic species. Atmos Chem Phys [Internet]. 2006 Sep 6;6(11):3625–4055. Available from: https://acp.copernicus.org/articles/6/3625/2006/

7. García MPGI, Sanroma AM, Porrero MPM, Valle AT, Galán BC, Muñoz MSS. Reactivity of 2-ethyl-1-hexanol in the atmosphere. Phys Chem Chem Phys. 2010;12(13):3294–300.

8. Maeng DY, McNeill VF. Kinetics of alkaline hydrolysis of synthetic organic esters. Int J

Chem Kinet. 2022;54(3):218–22.

9. Wolfe NL, Steen WC, Burns LA. Phthalate ester hydrolysis: Linear free energy relationships. Chemosphere. 1980;9(7–8):403–8.

10. Su G, Letcher RJ, Yu H. Organophosphate Flame Retardants and Plasticizers in Aqueous Solution: PH-Dependent Hydrolysis, Kinetics, and Pathways. Environ Sci Technol. 2016;50(15):8103–11.

11. Letinski DJ, Connelly MJ, Peterson DR, Parkerton TF. Slow-stir water solubility measurements of selected alcohols and diesters. Chemosphere. 2002;48(3):257–65.

12. Lin CC, Corsi RL. Texanol® ester alcohol emissions from latex paints: Temporal variations and multi-component recoveries. Atmos Environ. 2007;41(15):3225–34.

13. Bergh C, Torgrip R, Emenius G, Östman C. Organophosphate and phthalate esters in air and settled dust - a multi-location indoor study. Indoor Air. 2011;21(1):67–76.

14. Kortüm G, Vogel W, Andrussow K. Dissociation Constants of Organic Acids in Aqueous Solution. London: Butterworths; 1961.

15. Serjeant EP, Dempsey B. Ionisation Constants of Organic Acids in Aqueous Solution. Pergamon Press; 1979.

16. Lim HJ, Carlton AG, Turpin BJ. Isoprene forms secondary organic aerosol through cloud processing: Model simulations. Environ Sci Technol. 2005;39(12):4441–6.

17. Schwartz SE. Mass-Transport Considerations Pertinent to Aqueous Phase Reactions of Gases in Liquid-Water Clouds. In: Jaeschke W, editor. Chemistry of Multiphase

Atmospheric Systems [Internet]. Berlin, Heidelberg: Springer Berlin Heidelberg; 1986. p. 415–71. Available from: http://doi.wiley.com/10.1029/88EO00109

18. Tilgner A, Schaefer T, Alexander B, Barth M, Collett JL, Fahey KM, et al. Acidity and the multiphase chemistry of atmospheric aqueous particles and clouds. Atmos Chem Phys. 2021;21(17):13483–536.

19. Duncan SM, Sexton KG, Turpin BJ. Oxygenated VOCs, aqueous chemistry, and potential impacts on residential indoor air composition. Indoor Air. 2018;28(1):198–212.